

## Update on the Direct Detection of Dark Matter in MSSM Models with Non-Universal Higgs Masses

John Ellis<sup>1</sup>, Keith A. Olive<sup>2</sup> and Pearl Sandick<sup>3</sup>

<sup>1</sup>*TH Division, PH Department, CERN, CH-1211 Geneva 23, Switzerland*

<sup>2</sup>*William I. Fine Theoretical Physics Institute,  
University of Minnesota, Minneapolis, MN 55455, USA*

<sup>3</sup>*Theory Group and Texas Cosmology Center,  
The University of Texas at Austin, TX 78712, USA*

### Abstract

We discuss the possibilities for the direct detection of neutralino dark matter via elastic scattering in variants of the minimal supersymmetric extension of the Standard Model (MSSM) with non-universal supersymmetry-breaking contributions to the Higgs masses, which may be either equal (NUHM1) or independent (NUHM2). We compare the ranges found in the NUHM1 and NUHM2 with that found in the MSSM with universal supersymmetry-breaking contributions to all scalar masses, the CMSSM. We find that both the NUHM1 and NUHM2 offer the possibility of larger spin-independent dark matter scattering cross sections than in the CMSSM for larger neutralino masses, since they allow the density of heavier neutralinos with large Higgsino components to fall within the allowed range by astrophysics. The NUHM1 and NUHM2 also offer more possibilities than the CMSSM for small cross sections for lower neutralino masses, since they may be suppressed by scalar and pseudoscalar Higgs masses that are larger than in the CMSSM.

# 1 Introduction

Supersymmetry is one example of a theory that suggests the possibility of observing new particles at high-energy particle colliders such as the LHC. Many supersymmetric models predict that the lightest supersymmetric particle (LSP) should be stable and hence present in the Universe as a relic from the Big Bang [1]. As such, the LSP may provide all or some of the cold dark matter postulated by astrophysicists and cosmologists. In many supersymmetric models, the LSP is the lightest neutralino,  $\chi$ , though there are other possibilities such as the gravitino.

The most convincing vindication of any model of dark matter would be the direct detection of astrophysical dark matter particles via their scattering on nuclei in low-background experiments underground [2]. The model could then be further verified by comparing the direct dark matter detection rate with theoretical calculations based on measurements of the model parameters at colliders. If the LSP is indeed the lightest neutralino  $\chi$ , many estimates suggest that supersymmetric dark matter could be detected directly in present or forthcoming experiments [3–14]. On the other hand, if the LSP were the gravitino, the cross section for its scattering would be so small as to be undetectable.

Within the neutralino LSP scenario, the absence to date of supersymmetric signals in accelerator experiments imposes constraints on the possible direct detection rates. In general, these depend on the specific supersymmetric model, and specifically on the way in which supersymmetry is broken. We consider here the minimal supersymmetric extension of the Standard Model (MSSM) [15], and focus on three possibilities for the pattern of supersymmetry breaking.

In the simplest model the supersymmetry-breaking scalar masses  $m_0$  are constrained to be universal at some input GUT scale, a scenario called the CMSSM [16,17]. The absence of flavour-changing interactions beyond the Standard Model motivates the assumption that squarks or sleptons with the same quantum numbers should be (very nearly) degenerate [18], and universality between (some) squarks with different different quantum numbers and sleptons is suggested by some GUT models. These also suggest that the SU(3), SU(2) and U(1) gaugino masses  $m_{1/2}$  should be degenerate. The direct detection of neutralino dark matter within this CMSSM framework has been studied in many papers [4, 5, 7, 9–14].

However, there are no good reasons to expect universality for the supersymmetry-breaking contributions to the scalar masses of the MSSM Higgs multiplets. Accordingly, our main focus here is on variants of the MSSM with non-universal Higgs masses [19], generically called NUHM models. The supersymmetry-breaking contributions to the two Higgs masses might either be identical, a scenario called the NUHM1 [20,21], or might be different, a scenario we call the NUHM2 [22,23]. The direct detection of neutralino dark matter within the NUHM2 has also been studied in several papers [6, 13, 20], but direct detection within the NUHM1 has been less studied [20].

Since the amplitude for spin-independent dark matter scattering on a heavy nucleus receives important contributions from the exchanges of Higgs bosons, and since these are less constrained in NUHM models than in the CMSSM, *a priori* one would expect that the direct dark matter scattering cross section should exhibit more variability than in the CMSSM. In

particular, whereas the present experimental upper limits on dark matter scattering barely touch the range expected within the CMSSM, ongoing direct dark matter searches might already be sensitive to significant samples of NUHM models. Conversely, whereas the planned direct dark matter searches should be able to explore much of the CMSSM parameter space, it might be more likely that NUHM models could escape detection.

In this paper, we first review in Section 2 the relationships between the CMSSM, NUHM1 and NUHM2 models, as well as basic formulae underlying the calculation of the spin-independent and -dependent dark matter scattering cross sections. We then review briefly in Section 3 the expectations for direct dark matter detection within the CMSSM. Subsequently, we explore in Sections 4 and 5 the possible scattering cross sections in the NUHM1 and the NUHM2, respectively. These explorations each proceed in two steps: surveys of the variation in the direct dark matter cross section across some representative planes for fixed values of the other parameters, followed by a presentation and discussion of the overall range of possible values throughout the corresponding parameter space. We concentrate on spin-independent dark matter scattering because this seems closer to the present and likely experimental sensitivity than does spin-dependent scattering. Our conclusions are summarized in Section 6, where we comment on the possibilities for distinguishing experimentally between the CMSSM, NUHM1 and NUHM2.

## 2 Theoretical Framework

### 2.1 From the CMSSM to the NUHM1 and the NUHM2

The CMSSM has four continuous parameters and a sign that determine the weak-scale observables: the supposedly universal scalar mass  $m_0$ , gaugino mass  $m_{1/2}$  and universal trilinear coupling  $A_0$ ; the ratio of the Higgs vacuum expectation values,  $\tan\beta$ , and the sign of the Higgs mixing parameter  $\mu$ . The parameters  $m_0$ ,  $m_{1/2}$  and  $A_0$  and the sign of  $\mu$  are assumed to be specified at the GUT scale. A useful starting-point for analyzing the CMSSM is the  $(m_{1/2}, m_0)$  plane for some fixed value of  $A_0$ ,  $\tan\beta$  and sign of  $\mu$ . The input supersymmetry-breaking contributions to the effective Higgs masses-squared,  $m_{1,2}^2$  for the Higgs fields coupled to the down- and up-type quarks respectively, are renormalized differently below the GUT scale, because they are sensitive to different Yukawa couplings, specifically the  $t$ -quark coupling in the case of  $H_2$ , and this renormalization permits electroweak symmetry breaking at low energies. In the CMSSM,  $|\mu|$  and  $m_A$  are calculated from the electroweak vacuum conditions:

$$m_A^2(Q) = m_1^2(Q) + m_2^2(Q) + 2\mu^2(Q) + \Delta_A(Q) \quad (1)$$

and

$$\mu^2 = \frac{m_1^2 - m_2^2 \tan^2\beta + \frac{1}{2}m_Z^2(1 - \tan^2\beta) + \Delta_\mu^{(1)}}{\tan^2\beta - 1 + \Delta_\mu^{(2)}}, \quad (2)$$

where  $\Delta_A$  and  $\Delta_\mu^{(1,2)}$  are loop corrections [24–26],  $Q = (m_{\tilde{\tau}_R}m_{\tilde{\tau}_L})^{1/2}$ , and all quantities in (2) are defined at the electroweak scale,  $m_Z$ . Unless otherwise noted,  $m_A \equiv m_A(Q)$  and

$\mu \equiv \mu(m_Z)$ . The values of the parameters in (1) and (2) are related via

$$\begin{aligned} m_1^2(Q) &= m_1^2 + c_1, \\ m_2^2(Q) &= m_2^2 + c_2, \\ \mu^2(Q) &= \mu^2 + c_\mu, \end{aligned} \tag{3}$$

where  $c_1$ ,  $c_2$  and  $c_\mu$  are well-known radiative corrections [24, 27, 28].

The restriction  $m_1(M_{GUT}) = m_2(M_{GUT})$  is retained in the NUHM1, but these may differ from the otherwise universal scalar mass,  $m_0$ . The common GUT-scale value of the Higgs masses-squared therefore introduces an additional parameter in the NUHM1. This can be mapped into an additional free parameter in the effective low-energy theory, that may be taken to be either  $\mu$  or  $m_A$ . As in the CMSSM, one uses (1) - (3) to calculate the relationship between  $m_1^2$  and  $m_2^2$  at the weak scale that is required to respect the electroweak boundary conditions, allowing for the weakened universality condition at  $M_{GUT}$ . If  $m_A$  is taken to be the additional free low-energy parameter, then at  $m_Z$  we have [21]

$$\begin{aligned} m_1^2(\tan^2 \beta + 1 + \Delta_\mu^{(2)}) &= m_2^2(\tan^2 \beta + 1 - \Delta_\mu^{(2)}) + m_Z^2(\tan^2 \beta - 1) - 2\Delta_\mu^{(1)} \\ &+ (m_A^2 - (\Delta_A(Q) + c_1 + c_2 + 2c_\mu))(\tan^2 \beta - 1 + \Delta_\mu^{(2)}). \end{aligned} \tag{4}$$

Alternatively, if  $\mu$  is taken as the free parameter, then at  $m_Z$  we have

$$m_1^2 = m_2^2 \tan^2 \beta + \mu^2(\tan^2 \beta - 1 + \Delta_\mu^{(2)}) + \frac{1}{2}m_Z^2(\tan^2 \beta - 1) - \Delta_\mu^{(1)}. \tag{5}$$

In each case, the NUHM1 boundary condition at  $M_{GUT}$  is  $m_1^2 = m_2^2$ . Clearly, for some specific input values of  $\mu$  and  $m_A$ , one finds  $m_1^2(M_{GUT}) = m_2^2(M_{GUT}) = m_0^2$ , thereby recovering the CMSSM. The subject of Section 4 is the deviation from the CMSSM prediction for dark matter scattering that may be found in the NUHM1. We discuss first planar subspaces of the NUHM1 in which  $m_A$  is taken as the additional free low-energy parameter, and then consider planes with  $\mu$  as a free parameter.

In the NUHM2, the soft supersymmetry-breaking contributions to both the Higgs scalar masses  $m_{1,2}$  are regarded as free parameters. Correspondingly, these may be traded for free values of both  $\mu$  and  $m_A$  at low energies. In this case, we can write [22]

$$\begin{aligned} m_1^2(1 + \tan^2 \beta) &= m_A^2(Q) \tan^2 \beta - \mu^2(\tan^2 \beta + 1 - \Delta_\mu^{(2)}) - (c_1 + c_2 + 2c_\mu) \tan^2 \beta \\ &- \Delta_A(Q) \tan^2 \beta - \frac{1}{2}m_{\text{BZ}}^2(1 - \tan^2 \beta) - \Delta_\mu^{(1)} \end{aligned} \tag{6}$$

and

$$\begin{aligned} m_2^2(1 + \tan^2 \beta) &= m_A^2(Q) - \mu^2(\tan^2 \beta + 1 + \Delta_\mu^{(2)}) - (c_1 + c_2 + 2c_\mu) \\ &- \Delta_A(Q) + \frac{1}{2}m_{\text{BZ}}^2(1 - \tan^2 \beta) + \Delta_\mu^{(1)}. \end{aligned} \tag{7}$$

Each point in a CMSSM  $(m_{1/2}, m_0)$  plane can be ‘blown up’ into a  $(\mu, m_A)$  plane. The NUHM1 subspace may be represented as a line in such a  $(\mu, m_A)$  plane, and the CMSSM as one or two points on this line.

## 2.2 Dark Matter Scattering

The neutralino LSP  $\chi$  is the lowest-mass eigenstate combination of the Bino  $\tilde{B}$ , Wino  $\tilde{W}$  and neutral Higgsinos  $\tilde{H}_{1,2}$ . Its mass matrix  $N$  is diagonalized by a matrix  $Z$ :  $\text{diag}(m_{\chi_{1,\dots,4}}) = Z^* N Z^{-1}$ , and the composition of the lightest neutralino may be written as

$$\chi = Z_{\chi 1} \tilde{B} + Z_{\chi 2} \tilde{W} + Z_{\chi 3} \tilde{H}_1 + Z_{\chi 4} \tilde{H}_2. \quad (8)$$

The amplitude for  $\chi$  scattering on quarks depends on the squark mass-squared matrix, which is diagonalized by a matrix  $\eta$ :  $\text{diag}(m_1^2, m_2^2) \equiv \eta M^2 \eta^{-1}$ , which can be parameterized for each flavour  $f$  by an angle  $\theta_f$ <sup>1</sup>. The diagonalization matrix can be written as

$$\begin{pmatrix} \cos \theta_f & \sin \theta_f e^{i\gamma_f} \\ -\sin \theta_f e^{-i\gamma_f} & \cos \theta_f \end{pmatrix} \equiv \begin{pmatrix} \eta_{11} & \eta_{12} \\ \eta_{21} & \eta_{22} \end{pmatrix}. \quad (9)$$

The magnitudes of  $\mu$  and the pseudoscalar Higgs mass  $m_A$  are calculated using the appropriate electroweak vacuum conditions in the CMSSM, NUHM1 and NUHM2, as discussed in the previous Subsection.

The effective four-fermion Lagrangian relevant for relic dark matter scattering is [29]:

$$\mathcal{L} = \alpha_{2i} \bar{\chi} \gamma^\mu \gamma^5 \chi \bar{q}_i \gamma_\mu \gamma^5 q_i + \alpha_{3i} \bar{\chi} \chi \bar{q}_i q_i. \quad (10)$$

This Lagrangian is to be summed over the quark generations, and the subscript  $i$  labels up-type quarks ( $i = 1$ ) and down-type quarks ( $i = 2$ ). The coefficients are given by:

$$\begin{aligned} \alpha_{2i} &= \frac{1}{4(m_{1i}^2 - m_\chi^2)} [ |X_i|^2 + |Y_i|^2 ] + \frac{1}{4(m_{2i}^2 - m_\chi^2)} [ |W_i|^2 + |V_i|^2 ] \\ &\quad - \frac{g^2}{4m_Z^2 \cos^2 \theta_W} [ |Z_{\chi 3}|^2 - |Z_{\chi 4}|^2 ] \frac{T_{3i}}{2} \end{aligned} \quad (11)$$

and

$$\begin{aligned} \alpha_{3i} &= -\frac{1}{2(m_{1i}^2 - m_\chi^2)} \text{Re} [(X_i) (Y_i)^*] - \frac{1}{2(m_{2i}^2 - m_\chi^2)} \text{Re} [(W_i) (V_i)^*] \\ &\quad - \frac{gm_{q_i}}{4m_W B_i} \left\{ \left( \frac{D_i^2}{m_{H_2}^2} + \frac{C_i^2}{m_{H_1}^2} \right) \text{Re} [\delta_{2i} (gZ_{\chi 2} - g'Z_{\chi 1})] \right. \\ &\quad \left. + D_i C_i \left( \frac{1}{m_{H_2}^2} - \frac{1}{m_{H_1}^2} \right) \text{Re} [\delta_{1i} (gZ_{\chi 2} - g'Z_{\chi 1})] \right\}, \end{aligned} \quad (12)$$

where

$$\begin{aligned} X_i &\equiv \eta_{11}^* \frac{gm_{q_i} Z_{\chi 5-i}^*}{2m_W B_i} - \eta_{12}^* e_i g' Z_{\chi 1}^*, \\ Y_i &\equiv \eta_{11}^* \left( \frac{y_i}{2} g' Z_{\chi 1} + g T_{3i} Z_{\chi 2} \right) + \eta_{12}^* \frac{gm_{q_i} Z_{\chi 5-i}^*}{2m_W B_i}, \\ W_i &\equiv \eta_{21}^* \frac{gm_{q_i} Z_{\chi 5-i}^*}{2m_W B_i} - \eta_{22}^* e_i g' Z_{\chi 1}^*, \\ V_i &\equiv \eta_{21}^* \left( \frac{y_i}{2} g' Z_{\chi 1} + g T_{3i} Z_{\chi 2} \right) + \eta_{22}^* \frac{gm_{q_i} Z_{\chi 5-i}^*}{2m_W B_i}, \end{aligned} \quad (13)$$

<sup>1</sup>We ignore here all possible CP-violating phases.

where  $y_i, T_{3i}$  denote hypercharge and isospin, and

$$\delta_{1i} = Z_{\chi 3}(Z_{\chi 4}), \quad \delta_{2i} = Z_{\chi 4}(-Z_{\chi 3}), \quad (14)$$

$$B_i = \sin \beta (\cos \beta), \quad C_i = \sin \alpha (\cos \alpha), \quad D_i = \cos \alpha (-\sin \alpha) \quad (15)$$

for up (down) type quarks. We denote by  $m_{H_2} < m_{H_1}$  the masses of the two neutral scalar Higgs bosons, and  $\alpha$  denotes the neutral Higgs boson mixing angle.

In the NUHM1 and NUHM2, the greater freedom in the choice(s) of the input values of  $m_1^2$  and  $m_2^2$  translates into greater freedom for  $m_{H_2}$  and  $m_{H_1}$  than in the CMSSM and hence, *a priori*, more variation in the dark matter scattering amplitude.

The elastic cross section for  $\chi$  scattering on a nucleus can be decomposed into a scalar (spin-independent) part obtained from  $\alpha_{3i}$  (12), and a spin-dependent part obtained from  $\alpha_{2i}$  (11). Each of these can be written in terms of the cross sections for elastic scattering off individual nucleons, as we now review.

The scalar, or spin-independent (SI), part of the cross section can be written as <sup>2</sup>

$$\sigma_{\text{SI}} = \frac{4m_r^2}{\pi} [Zf_p + (A - Z)f_n]^2, \quad (16)$$

where  $m_r$  is the  $\chi$ -nuclear reduced mass and

$$\frac{f_N}{m_N} = \sum_{q=u,d,s} f_{T_q}^{(N)} \frac{\alpha_{3q}}{m_q} + \frac{2}{27} f_{TG}^{(N)} \sum_{q=c,b,t} \frac{\alpha_{3q}}{m_q} \quad (17)$$

for  $N = p$  or  $n$ . The parameters  $f_{T_q}^{(N)}$  are defined by

$$m_N f_{T_q}^{(N)} \equiv \langle N | m_q \bar{q}q | N \rangle \equiv m_q B_q^{(N)}, \quad (18)$$

where [31, 32]

$$f_{TG}^{(N)} = 1 - \sum_{q=u,d,s} f_{T_q}^{(N)}. \quad (19)$$

We take the central ratios of the light quark masses from [33]:

$$\frac{m_u}{m_d} = 0.553, \quad \frac{m_s}{m_d} = 18.9. \quad (20)$$

We take the other quark masses from [34], except for the top mass, which is taken from the combined CDF and D0 result [35].

Following [36], we introduce the quantity:

$$z \equiv \frac{B_u^{(p)} - B_s^{(p)}}{B_d^{(p)} - B_s^{(p)}} = 1.49, \quad (21)$$

---

<sup>2</sup>This expression is valid in the zero-momentum-transfer limit. For non-zero momentum exchange, the expression must include a form factor due to the finite size of the nucleus. See, for example, Ref. [30].

which has an experimental error that is negligible compared with others in this calculation, and the strange scalar density

$$y \equiv \frac{2B_s^{(N)}}{B_u^{(N)} + B_d^{(N)}}. \quad (22)$$

In terms of these, one may write

$$\frac{B_d^{(p)}}{B_u^{(p)}} = \frac{2 + ((z - 1) \times y)}{2 \times z - ((z - 1) \times y)}. \quad (23)$$

Proton and neutron scalar matrix elements are related by an interchange of  $B_u$  and  $B_d$ , i.e.,

$$B_u^{(n)} = B_d^{(p)}, \quad B_d^{(n)} = B_u^{(p)}, \quad \text{and} \quad B_s^{(n)} = B_s^{(p)}. \quad (24)$$

The  $\pi$ -nucleon sigma term,  $\Sigma_{\pi N}$ , may be written as

$$\Sigma_{\pi N} \equiv \frac{1}{2}(m_u + m_d) \times (B_u^{(N)} + B_d^{(N)}), \quad (25)$$

and the coefficients  $f_{T_q}$  may be written in the forms [14]:

$$f_{T_u} = \frac{m_u B_u}{m_N} = \frac{2\Sigma_{\pi N}}{m_N(1 + \frac{m_d}{m_u})(1 + \frac{B_d}{B_u})}, \quad (26)$$

$$f_{T_d} = \frac{m_d B_d}{m_N} = \frac{2\Sigma_{\pi N}}{m_N(1 + \frac{m_u}{m_d})(1 + \frac{B_u}{B_d})}, \quad (27)$$

$$f_{T_s} = \frac{m_s B_s}{m_N} = \frac{(\frac{m_s}{m_d})\Sigma_{\pi N} y}{m_N(1 + \frac{m_u}{m_d})}; \quad (28)$$

where we have dropped the  $(N)$  superscript from  $f_{T_q}$  and  $B_q$ .

The value of  $y$  is related to the  $\pi$ -nucleon sigma term  $\Sigma_{\pi N}$  by

$$y = 1 - \sigma_0/\Sigma_{\pi N}. \quad (29)$$

The central value for  $\sigma_0$  is estimated on the basis of octet baryon mass differences to be  $\sigma_0 = 36$  MeV [37–40], and the latest determination of  $\Sigma_{\pi N} = 64$  MeV. These are the values assumed in our analyses of the CMSSM, NUHM1 and NUHM2: the effect of varying these assumptions are discussed in the context of the CMSSM in [13,14]. *We take this opportunity to reiterate the importance of measuring  $\Sigma_{\pi N}$  as accurately as possible [14]*<sup>3</sup>.

The spin-dependent (SD) part of the elastic  $\chi$ -nucleus cross section can be written in the zero momentum transfer limit as

$$\sigma_{SD} = \frac{32}{\pi} G_F^2 m_r^2 \Lambda^2 J(J + 1), \quad (30)$$

---

<sup>3</sup>Lattice calculations are now reaching the stage where they may also provide useful information on  $\Sigma_{\pi N}$  [41].

where  $m_r$  is again the reduced neutralino mass,  $J$  is the spin of the nucleus, and

$$\Lambda \equiv \frac{1}{J} (a_p \langle S_p \rangle + a_n \langle S_n \rangle) , \quad (31)$$

where

$$a_p \equiv \sum_q \frac{\alpha_{2q}}{\sqrt{2}G_f} \Delta_q^{(p)} , \quad a_n \equiv \sum_i \frac{\alpha_{2q}}{\sqrt{2}G_f} \Delta_q^{(n)} . \quad (32)$$

The factors  $\Delta_q^{(N)}$  parametrize the quark spin content of the nucleon and are only significant for the light (u,d,s) quarks. For definiteness, we assume

$$\Delta_u^{(p)} = 0.84 , \Delta_d^{(p)} = -0.43 , \Delta_s^{(p)} = -0.09 . \quad (33)$$

The effects of varying these assumptions are also discussed in the context of the CMSSM in [14].

### 3 CMSSM Models

We begin with a brief discussion of detection prospects in the CMSSM. In panel (a) of Fig. 1, we show the  $(m_{1/2}, m_0)$  plane for  $\tan \beta = 10$ ,  $A_0 = 0$ , and  $\mu > 0$ . The region excluded because the LSP is a charged  $\tilde{\tau}$  is shaded brown, and that where electroweak symmetry breaking cannot be obtained, resulting in unphysical  $\mu^2 < 0$ , in dark pink. The red dot-dashed contour corresponds to a Higgs mass of 114 GeV. At lower  $m_{1/2}$  the Higgs boson would be lighter, which is excluded by its non-observation at LEP [42]. We also plot a black dashed contour for  $m_{\chi^\pm} = 104$  GeV, the region at lower  $m_{1/2}$  also being excluded by LEP. The green shaded region at very low  $m_{1/2}$  and  $m_0$  is disfavored by the measured branching ratio for  $b \rightarrow s\gamma$  [43], while the light pink shaded region is favored by the measurement of the muon anomalous magnetic moment at the 2- $\sigma$  level [44]. Finally, in the turquoise shaded regions, the relic density of neutralinos falls within the WMAP range [45]. For the value  $\tan \beta = 10$  used here, the only cosmologically-preferred regions are the coannihilation strip, bordering the  $\tilde{\tau}$ -LSP region, and the focus-point region at large  $m_0$ , where  $\mu$  is small and the LSP is a mixed bino-Higgsino state. Over the bulk of the plane, the relic density of neutralinos exceeds the WMAP range by more than 2  $\sigma$ . There are, however, slim strips where  $\Omega_\chi h^2$  is below the WMAP range, which lie between the strips of good relic density and the excluded regions they border. These portions of the plane are not forbidden, as there could be some additional source of cold dark matter.

In panel (b) of Fig. 1 we show the neutralino-nucleon elastic scattering cross sections as functions of neutralino mass for the regions of panel (a) that are cosmologically viable (i.e., those where the upper limit on the relic density of neutralinos is respected), and are not excluded by constraints from colliders. We also plot the limits on the spin-independent cross section from CDMS II [46] (solid black line) and XENON10 [47] (solid red line), as well as the sensitivities projected for XENON100 [48] (or a similar 100-kg liquid noble-gas detector such as LUX, dashed red line) and SuperCDMS at the Soudan Mine [49] (dashed black line). We do not show the experimental bound for the spin-dependent scattering of a neutralino



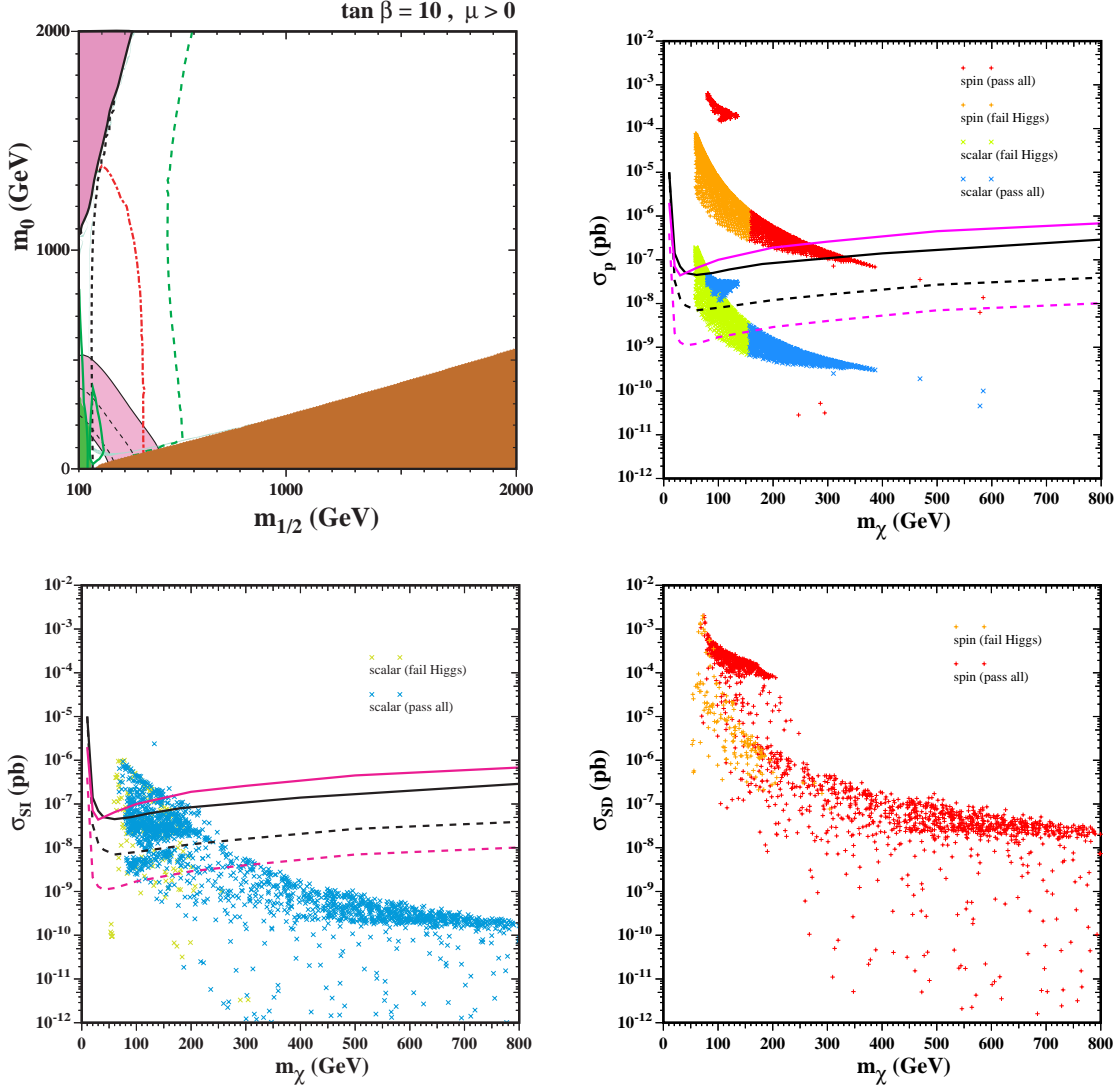


Figure 1: Panels (a) and (b) show the CMSSM  $(m_{1/2}, m_0)$  plane and the corresponding cosmologically viable neutralino-nucleon elastic scattering cross sections as functions of neutralino mass for  $\tan \beta = 10$  and  $A_0 = 0$ . Panel (c) shows the entire potential range of neutralino-nucleon cross sections as functions of neutralino mass for the CMSSM, with  $5 \leq \tan \beta \leq 55$ ,  $0 \leq m_{1/2} \leq 2000$  GeV,  $100$  GeV  $\leq m_0 \leq 2000$  GeV, and  $-3m_{1/2} \leq A_0 \leq 3m_{1/2}$ . We consider  $\mu < 0$  only for  $\tan \beta < 30$ . Also shown are upper limits on the spin-independent dark matter scattering cross section from CDMS II [46] (solid black line) and XENON10 [47] (solid pink line), as well as the expected sensitivities for XENON100 [48] (dashed pink line) and SuperCDMS at the Soudan Mine [49] (dashed black line).

on a proton as the current best limit is 0.2 pb (at  $m_\chi = 100$  GeV) [50] and is off the scale of our plot. The limit for the scattering on neutrons is stronger but is still only at the level of 0.02 pb [46].

When stating limits or projections, direct detection experiments assume as a prior that  $\Omega_{WIMP} = \Omega_{CDM}$ , where  $\Omega_{CDM}$  is that measured by WMAP. If  $\Omega_{WIMP} < \Omega_{CDM}$ , we assume that the rest of the cold dark matter is due to some other source, and we rescale the plotted neutralino-nucleon cross sections by a factor  $\Omega_\chi/\Omega_{CDM}$ , so that comparison with direct searches is possible.

In panel (b), we display both the spin-dependent and spin-independent (scalar) cross sections for neutralino-nucleon elastic scattering. In each case, there are two distinct regions in the  $(M_\chi, \sigma)$  plane, that arising from the focus-point region at  $m_\chi \lesssim 150$  GeV and relatively large  $\sigma$ , and that from the coannihilation strip. In the coannihilation strip,  $50 \text{ GeV} < m_\chi < 400 \text{ GeV}$ , where the lower limit on  $m_\chi$  is a result of the LEP constraint on the chargino mass, and the upper limit on  $m_\chi$  corresponds to the end-point of the coannihilation strip for  $\tan\beta = 10$ . In contrast, the end point of the focus-point region shown is due only to the cut-off  $m_0 < 2$  TeV that we assume.

In addition, for  $m_{1/2} \lesssim 380$  GeV in the coannihilation strip ( $m_\chi \lesssim 160$  GeV), the nominal calculated mass of the lighter scalar MSSM Higgs boson is less than the LEP lower bound. These points are indicated by lighter shadings: lime green for the spin-independent scattering cross sections, and ochre for the spin-dependent scattering cross sections<sup>4</sup>. In general, such points may not be strictly forbidden, as the calculated mass<sup>5</sup> has a theoretical uncertainty estimated as 1.5 GeV, and the MSSM Higgs has slightly different couplings from the SM Higgs for which the LEP limit was set. However, in the CMSSM the couplings are generally very close and (up to theoretical and experimental uncertainties) the limit should hold in this case.

At very low  $m_{1/2}$ , CDMS II and XENON10 have definitively excluded some of the region where  $m_h$  is below the LEP limit. We show this explicitly in panel (a), by plotting the reach of current and future direct detection experiments in the supersymmetric parameter space. Here and in subsequent parameter space scans, we display contours of the scalar neutralino-nucleon cross section, scaled by  $\Omega_\chi/\Omega_{CDM}$  if necessary, of  $5 \times 10^{-8}$  pb (solid green lines) and  $10^{-9}$  pb (dashed green lines). A cross section of  $5 \times 10^{-8}$  pb is currently excluded by XENON10 for  $m_\chi = 30$  GeV and by CDMS II for  $m_\chi = 60$  GeV, and will be probed by SuperCDMS for  $m_\chi$  up to  $\sim 1000$  GeV. Tonne-scale liquid noble-gas detectors such as the proposed XENON1T or a similar detector mass for LUX/ZEP will be sensitive to scalar cross sections below  $10^{-9}$  pb for all neutralino masses in the range  $10 \text{ GeV} \lesssim m_\chi \lesssim$  a few TeV [48]. Indeed, they will be sensitive to cross sections below  $10^{-10}$  pb over much of the preferred mass range  $m_\chi \sim O(100)$  GeV.

The choices  $\tan\beta = 10$  and  $A_0 = 0$  do not yield viable direct detection cross sections that are completely representative of the range of possibilities within the CMSSM. Therefore, in panels (c) and (d) of Fig. 1 we show CMSSM spin-independent and spin-dependent neutralino-nucleon cross sections, respectively, as obtained in a scan over all CMSSM pa-

<sup>4</sup>Note that in the focus-point region the calculated Higgs mass always exceeds the LEP lower limit.

<sup>5</sup>We use FeynHiggs [51] to calculate the Higgs mass.

parameters with  $5 \leq \tan\beta \leq 55$ ,  $0 \leq m_{1/2} \leq 2000$  GeV,  $100$  GeV  $\leq m_0 \leq 2000$  GeV, and  $-3m_{1/2} \leq A_0 \leq 3m_{1/2}$ . We also allow both positive and negative  $\mu$ , except for large  $\tan\beta > 30$ , where convergence becomes difficult in the  $\mu < 0$  case <sup>6</sup>.

For future reference, we note the ranges of CMSSM cross sections for different given neutralino masses. At low  $m_\chi < 300$  GeV, cross sections generally exceed  $10^{-9}$  pb, and the largest scalar cross sections, which occur for  $m_\chi \sim 100$  GeV, are already excluded by XENON10 and/or CDMS II <sup>7</sup>. These exclusions occur primarily in the focus-point region at large  $\tan\beta$ . On the other hand, for  $m_\chi \gtrsim 400$  GeV scalar cross sections are well below  $10^{-9}$  pb, and come from the coannihilation strip or the rapid-annihilation funnel that appears at large  $\tan\beta$  in the CMSSM <sup>8</sup>. Moreover, the effective cross sections are suppressed for points with  $\Omega_\chi \ll \Omega_{CDM}$ , and there may be cancellations at larger  $m_\chi$  that suppress the cross sections substantially. These regions of parameter space will not be probed by direct detection experiments in the near future.

## 4 NUHM1 Models

In NUHM1 models, either  $\mu$  or  $m_A$  may be taken as a free parameter, in addition to the four parameters and  $\mu$  sign choice in the CMSSM. To examine the parameter space, we may choose to fix either  $m_{1/2}$  or  $m_0$ , along with  $\tan\beta$ ,  $A_0$ , and the sign of  $\mu$ , and perform a scan over the remaining two parameters [21].

Before exploring the NUHM1 parameter space, we first make some general comments. The LSP may be either bino-like or a mixed bino-Higgsino state. If the LSP is bino-like, its mass is nearly equal to the bino mass,  $M_1$ , which is proportional to  $m_{1/2}$ :  $m_\chi \sim 0.42m_{1/2}$  for a bino-like neutralino. Scans with fixed  $m_{1/2}$  can therefore provide only limited information on the accessibility of the full parameter space with direct dark matter detection experiments. When  $\mu$  becomes less than  $M_1$ , however, the LSP becomes increasingly Higgsino-like, and its mass is strongly influenced by the value of  $\mu$ . Specifically, one finds that the mass drops off as the Higgsino component becomes more substantial.

### 4.1 Exploring Large $m_0$ in Sample NUHM1 Planes

We display in Fig. 2 representative NUHM1  $(m_A, m_0)$  and  $(\mu, m_0)$  planes in panels (a) and (c), and the corresponding neutralino-nucleon elastic scattering cross sections as functions of the neutralino mass for cosmologically viable regions of the NUHM1 plane in panels (b) and (d), respectively. Although fixing  $m_{1/2}$  limits the range of neutralino masses, as already commented, and hence also the cross sections, the  $(m_A, m_0)$  and  $(\mu, m_0)$  planes in panels (a) and (c) of Fig. 2 exhibit many of the constraints and features that provide the basis for understanding direct detection prospects in models with non-universal Higgs masses

---

<sup>6</sup>We recall that models with  $\mu < 0$  are generally disfavoured by  $g_\mu - 2$ , but we do not use this as a restriction on our parameter scans.

<sup>7</sup>These results are consistent with those presented in [13].

<sup>8</sup>Bordering these regions, the relic density of neutralinos can be quite low with respect to  $\Omega_{CDM}$  such that some of the cross sections in panels (c) and (d) are highly scaled.

discussed in the following sections. In panel (a), for example, regions of the plane at very low  $m_A$  are excluded because the lighter scalar Higgs mass falls below the LEP bound (red dot-dashed line) and/or  $\text{BR}(b \rightarrow s\gamma)$  is too large (green shading). At large  $m_A$  relative to  $m_0$ , it becomes impossible to satisfy the electroweak vacuum conditions with a real value of  $\mu$ , leading to the pink unphysical region. The brown and black regions at very low  $m_0$  are forbidden because they have a stau or selectron/smuon LSP, respectively.

There are four distinct regions in panel (a) of Fig. 2 where the relic density of neutralinos falls within the WMAP range. At low  $m_A$  and  $m_0$ , the selectron and stau are nearly degenerate, and both are lighter than the lightest neutralino, with the selectron being the lighter. Close to this forbidden region, there is an allowed turquoise strip where *coannihilations* of neutralinos with selectrons and staus bring the relic density down into the WMAP range. Near  $m_A = 420$  GeV, where  $m_A = 2m_\chi$  as indicated by the solid blue line, a *rapid-annihilation funnel* rises out of the coannihilation strip. Between the two funnel walls where  $2m_\chi \approx m_A$ , the relic density of neutralinos is brought below the WMAP range by an enhanced annihilation rate through the direct-channel  $A$  pole. On the other side of the funnel, we see a continuation of the coannihilation strip, near the border of the region where the stau is the LSP. The final region where the relic density of neutralinos falls within the WMAP range occurs along the border of the unphysical region at large  $m_A$  where electroweak symmetry breaking cannot be obtained, in the *focus-point region*. Here, as  $\mu \rightarrow 0$ , the LSP becomes increasingly Higgsino-like, and annihilations to gauge bosons are enhanced. Since  $m_{1/2} = 500$  GeV in this plane, the LSP is bino-like with a mass of just over 200 GeV in all cosmologically viable regions except the focus-point region, where the mass of the lightest neutralino depends on  $\mu$  and may be smaller.

As a result, panel (b) shows cross sections possible in this plane as a strip at  $m_\chi \sim 200$  GeV, including values in both the coannihilation strip and the rapid-annihilation funnel, where the LSP is bino-like and  $m_\chi \sim 0.42m_{1/2}$ . We note that there are points with  $m_\chi \sim 210$  GeV that have very low cross sections because they lie in the rapid-annihilation funnel at large  $m_0$ , a possibility offered in the NUHM1 because of the freedom in the Higgs masses, that was absent in the CMSSM. On the other hand, the focus-point region yields the largest cross sections. However, as the LSP becomes increasingly Higgsino-like, its mass decreases with  $\mu$ , and the relic density eventually falls below the WMAP range. Thus, we rescale the cross sections at lower  $m_\chi$  by a factor of  $\Omega_\chi/\Omega_{\text{WMAP}}$ , which decreases as the Higgsino fraction increases and  $\Omega_\chi$  decreases. Had a larger (smaller) value of  $m_{1/2}$  been chosen, these features in panel (b) would have been shifted to larger (smaller)  $m_\chi$ .

The green dot-dashed line in panel (a) marks the CMSSM subspace within this NUHM1 plane. It crosses the cosmologically viable regions in two places: at large  $(m_A, m_0)$  in the focus-point region, and at low  $m_0$  in the stau coannihilation strip. The largest CMSSM cross sections of a few  $\times 10^{-8}$  pb come from the focus-point region, as already seen in Fig. 1, whereas cross sections from CMSSM points along the coannihilation strip peak at  $\sim 10^{-9}$  pb. Moreover, they are rescaled in the portion of the CMSSM contour that extends into the area below the coannihilation strip, where the relic density of neutralinos can be as much as an order of magnitude below the WMAP range.

Panel (c) shows an NUHM1  $(\mu, m_0)$  plane, again with  $m_{1/2}$  fixed to be 500 GeV. Many

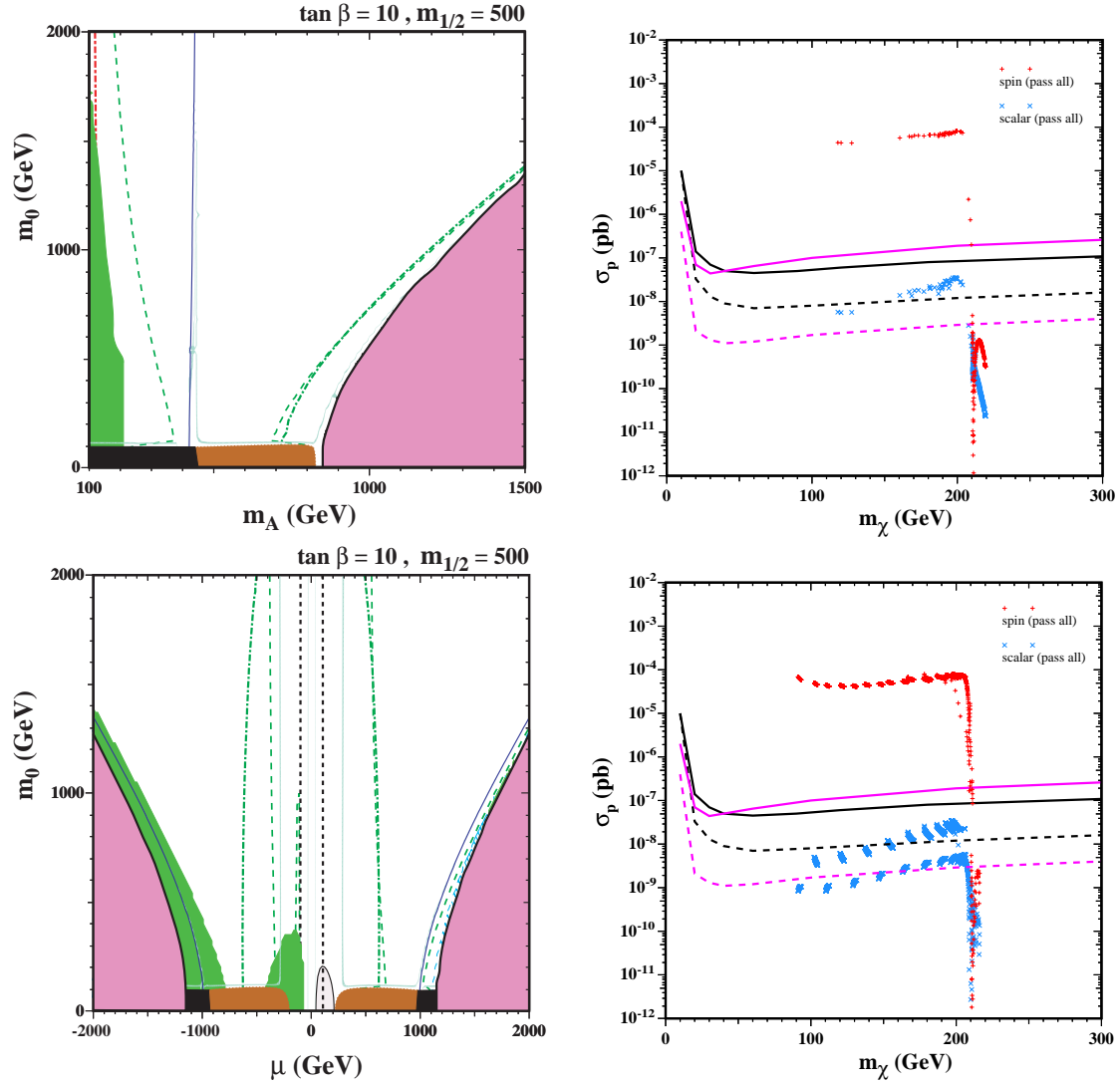


Figure 2: Panels (a) and (c) show the NUHM1 ( $m_A, m_0$ ) and ( $\mu, m_0$ ) planes for  $m_{1/2} = 500$  GeV,  $\tan \beta = 10$ , and  $A_0 = 0$  ( $\mu > 0$  in panel (a)). Panels (b) and (d) show the corresponding neutralino-nucleon elastic scattering cross sections for cosmologically-viable models as functions of neutralino mass.

of the features mentioned above are also present in panel (c). Note that there is a small region with  $100 \text{ GeV} < \mu < 200 \text{ GeV}$  and  $m_0 < 200 \text{ GeV}$  that may be favoured by  $g_\mu - 2$  (light pink shading, bounded by solid black line). There are rapid-annihilation funnels and coannihilation strips at both positive and negative  $\mu$ . Also, at large  $|\mu|$  there are unphysical regions where the electroweak vacuum conditions imply  $m_A^2 < 0$ , and the rapid-annihilation funnels, where  $m_A \sim 420 \text{ GeV}$ , run close to these borders. There is also an analogue of the focus-point region in the form of *crossover strips* of good relic density at  $|\mu| \sim 300 \text{ GeV}$ , where the LSP has a substantial Higgsino component. The  $\text{BR}(b \rightarrow s\gamma)$  constraint is important primarily for  $\mu < 0$ , shown in the left half-plane of (c), in which case it excludes the funnel and parts of the coannihilation and crossover strips. The LEP constraint on the Higgs mass is insignificant in panel (c), as is the upper limit on  $\text{BR}(B_s \rightarrow \mu^+ \mu^-)$ , which becomes important only at larger  $\tan\beta$ . The green dot-dashed CMSSM contours run roughly vertically at  $|\mu| \sim 500\text{-}600 \text{ GeV}$ , and in the visible part of the plane they intersect only the cosmologically preferred coannihilation strips at low  $m_0$ . However, at larger  $m_0$  the CMSSM contours would join together to form a parabola, and intersect the crossover strips at both positive and negative  $\mu$ , outside the visible part of the plane. In the area between the crossover strips, the relic density of neutralinos is below the WMAP range, resulting in rescaled cross sections in panel (d) that decrease for the increasingly Higgsino-like LSPs at lower  $m_\chi$ . There are two distinct strips of scalar cross sections in panel (d) for Higgsino-like LSPs: the upper one corresponding to  $\mu > 0$ , and the lower to  $\mu < 0$ . Cross sections for  $\mu < 0$  are suppressed by cancellations in the scattering matrix element due to sign differences in the neutralino eigenvectors.

We illustrate in panels (b) and (d) the reaches of current and future direct detection experiments in the NUHM1 parameter space. As can be seen from the green dashed contours of  $\sigma_{SI}$  drawn in panel (a), probing this plane will require a sensitivity below  $5 \times 10^{-8} \text{ pb}$ . In particular, to probe the coannihilation strip at low  $m_A$  and all of the focus-point region would require a direct detection experiment with a sensitivity of  $10^{-9} \text{ pb}$ . For the  $(\mu, m_0)$  plane in panel (c),  $10^{-9} \text{ pb}$  would again suffice to probe the phenomenologically viable region between the crossover strips<sup>9</sup> as well as some of the coannihilation strip. Unfortunately, scalar neutralino-nucleon elastic scattering cross sections in the rapid-annihilation funnel regions of both panels (a) and (c) may be considerably lower, as these points may have very large values of  $m_0$  - a feature not found in the CMSSM. Only a detector like LUX/ZEP with 20 tonnes would have sufficient sensitivity to probe also the funnel.

Fig. 3 shows corresponding  $(m_A, m_0)$  and  $(\mu, m_0)$  planes with  $\tan\beta = 10$  and a lower value of  $m_{1/2} = 300 \text{ GeV}$  close to the best fit value for the NUHM1 found in [52]. Comparing its panel (a) with that of Fig. 2, we see that the electroweak symmetry breaking constraint is more important, as is the Higgs mass constraint, whereas the  $b \rightarrow s\gamma$  constraint is less important. A new feature is that a region at low  $m_0$  is apparently favoured by  $g_\mu - 2$ . We also note that the prospective reach of future searches for spin-independent dark matter scattering in the  $(m_A, m_0)$  plane is considerably greater for  $m_{1/2} = 300 \text{ GeV}$  than for  $m_{1/2} =$

<sup>9</sup>Within the region at very low  $|\mu|$  where the chargino mass is below the LEP bound, we omit the contours of  $\sigma_{SI} = 10^{-9} \text{ pb}$ . The relic density of neutralinos can be quite low in this region, such that  $10^{-9} \text{ pb}$  is not sufficient to probe the entirety of this already-excluded strip.

500 GeV, as seen by the shift in the green dashed contour between the corresponding panels (a) <sup>10</sup>. However, as seen in panel (b), there is no large increase in the spin-independent dark matter scattering cross section in the regions of the plane allowed by WMAP, and the points with larger cross sections, most of which have  $m_\chi \sim 120$  GeV or less, generally have  $m_h < 114$  GeV. We also note that there are points with  $m_\chi \sim 120$  GeV and very low cross sections, due again to their locations at large  $m_0$  along the rapid-annihilation funnel in panel (a).

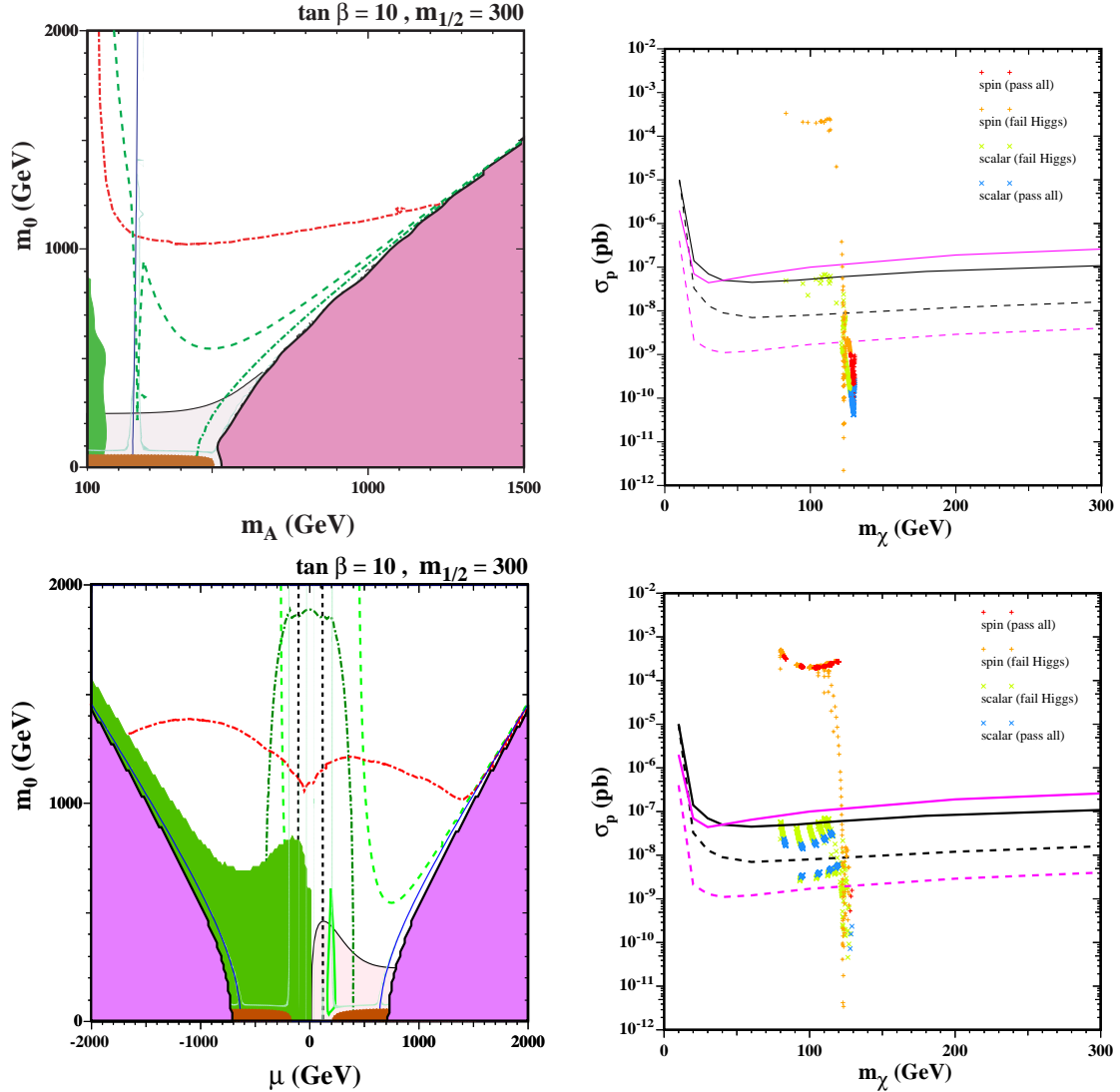


Figure 3: As in Fig. 2, but for  $m_{1/2} = 300$  GeV.

<sup>10</sup>The dip around  $m_A = 280$  GeV in Fig. 3(a) is due to the rescaling of the cross section in the underdense band between the rapid-annihilation strips.

Comparing the  $(\mu, m_0)$  plane in Fig. 3(c) with that in panel (c) of Fig. 2, we again see increased importance for the electroweak vacuum and LEP Higgs constraints, and the  $b \rightarrow s\gamma$  constraint for  $\mu < 0$  is also more important. We also note the appearance of a region at low  $m_0$  that is apparently favoured by  $g_\mu - 2$ , and that the prospective reach of future searches for spin-independent dark matter scattering in the  $(m_A, m_0)$  plane is again considerably greater for  $m_{1/2} = 300$  GeV than for  $m_{1/2} = 500$  GeV. As in panel (b) of Fig. 3, only a few points in panel (d) escape the LEP Higgs constraint, but some of these are in the focus-point region with  $m_\chi < 120$  GeV, and have spin-independent scattering cross sections close to the present experimental upper limits. We again see points with  $m_\chi \sim 120$  GeV and very low cross sections, that lie along the rapid-annihilation funnel in panel (c), at large  $m_0$ . These points have no counterparts in the CMSSM.

After these exploratory studies introducing some properties of characteristic dark matter regions, we next study more systematically NUHM1 planes with  $m_{1/2}$  and either  $m_A$  or  $\mu$  as free parameters, keeping  $m_0$  fixed.

## 4.2 The NUHM1 with $m_A$ as a free parameter

Fig. 4(a) displays a  $(m_A, m_{1/2})$  plane with fixed  $\tan\beta = 10, m_0 = 500$  GeV. The triangular allowed region is bounded by  $b \rightarrow s\gamma$  at small  $m_A$ , the appearance of a slepton LSP at large  $m_{1/2}$ , and the absence of a consistent electroweak vacuum at larger  $m_A$  and smaller  $m_{1/2}$ . The diagonal blue line indicates where  $m_\chi = m_A/2$ : on either side there is a narrow rapid-annihilation funnel strip where the relic density falls within the WMAP range. This funnel extends only to  $m_{1/2} \approx 1200$  GeV, and therefore  $m_\chi \lesssim 550$  GeV for this region. There is another WMAP strip in the focus-point region close to the electroweak vacuum boundary, where the LSP is more Higgsino-like. The displayed part of the focus-point strip is cut off at  $m_A = 2000$  GeV, corresponding to  $m_\chi \lesssim 600$  GeV: larger values of  $m_\chi$  would be allowed if one considered larger values of  $m_A$ . Apart from the region between this strip and the boundary, and between the funnel strips, the relic LSP density would exceed the WMAP range. The green dot-dashed CMSSM contour runs only through regions excluded either by excessive  $\Omega_\chi h^2$  or by the LEP chargino mass limit. Whilst the  $\text{BR}(b \rightarrow s\gamma)$  limit is also important at very low  $m_A$  and  $m_0$ , it is the constraint on the Higgs mass (shown by the red dot-dashed curve that is roughly horizontal at  $m_{1/2} = 400$  GeV) that places a lower limit on the expected LSP mass for the funnel region of  $m_\chi \sim 160$  GeV, where the LSP is bino-like.

We see in panel (a) that the green dashed line indicating future sensitivity to spin-independent dark matter scattering is mainly in the region where the relic density exceeds the WMAP upper limit. SuperCDMS at Soudan would be sensitive to much of the focus-point region shown in panel (a), but a more advanced detector would be required if the relic density of neutralinos is below the WMAP range. Unfortunately, even if neutralinos make up all the dark matter in the universe, much of the funnel region will remain out of reach, even to next-generation direct detection experiments. Points associated with the funnel with cross sections larger than  $10^{-9}$  pb fail the Higgs mass constraint.

Panel (b) of Fig. 4 displays the scattering cross sections for the allowed points in panel (a). The fact that scalar cross sections in the funnel region are generally smaller than those



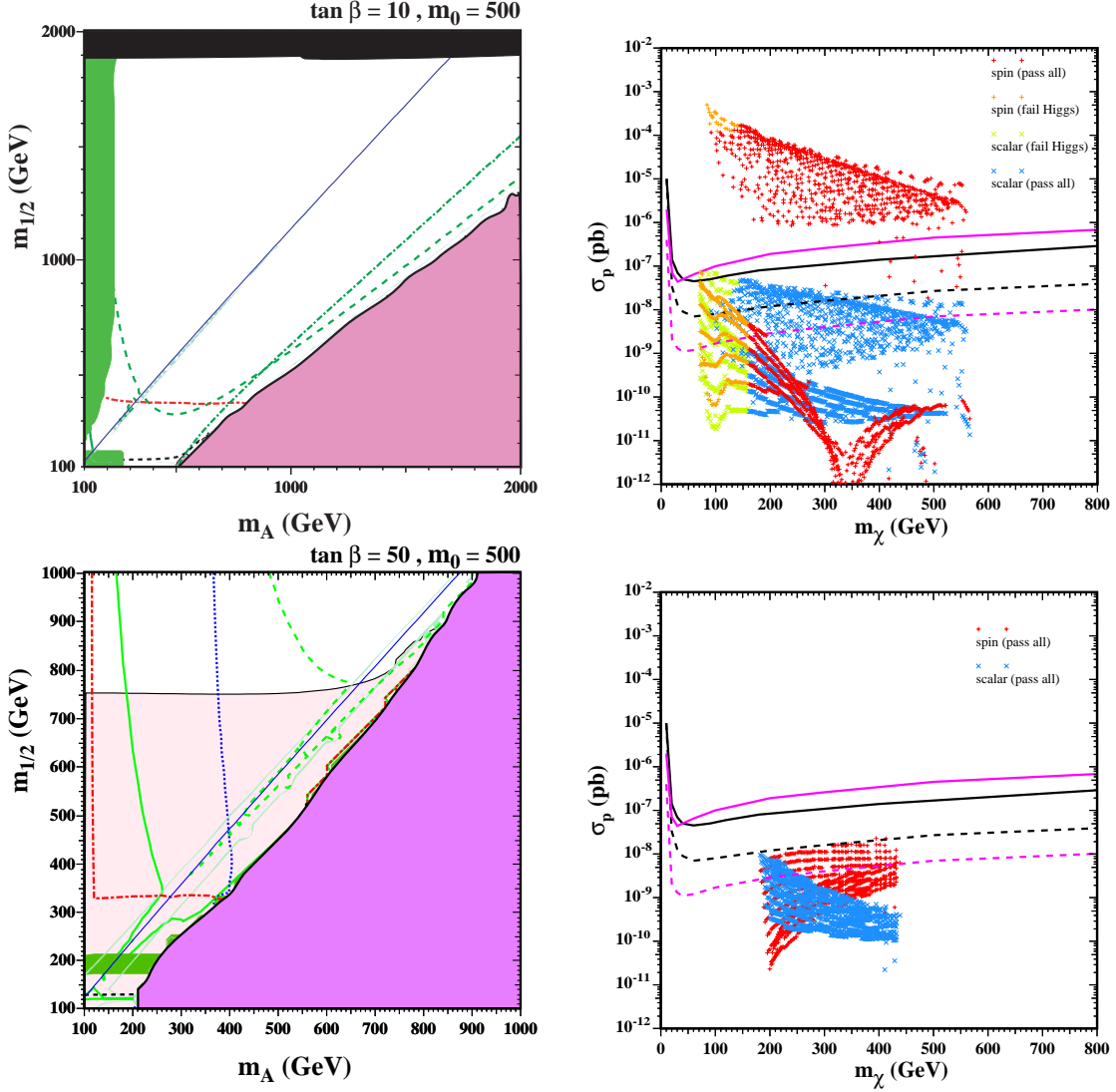


Figure 4: Panels (a) and (c) show the NUHM1  $(m_A, m_{1/2})$  planes for  $m_0 = 500$  GeV,  $\tan \beta = 10$  and 50. Panels (b) and (d) show the corresponding neutralino-nucleon elastic scattering cross sections as functions of neutralino mass.

in the focus-point region is reflected in the lower cutoff on the LSP mass,  $m_\chi \lesssim 550$  GeV, seen in panel (b) for the points with  $\sigma_{SI} \lesssim \text{few} \times 10^{-10}$  pb. In the focus-point region the LSP is in a mixed state  $m_\chi \lesssim 600$  GeV, and the cross section may be much larger: by two orders of magnitude for the spin-independent cross section, and four orders of magnitude for the spin-dependent cross section. These large cross sections at large  $m_\chi$  have no counterparts in the CMSSM, since in that model mixed states in the focus-point region have much lower masses. Furthermore, in the CMSSM, the focus point is reached only at large  $m_0$ , whereas

here,  $m_0 = 500$  GeV is fixed. The large scalar cross sections in the focus-point region are already beginning to be probed by CDMS II and XENON10, with a few points at very low  $m_{1/2}$  already being excluded, as one can see directly in panel (b) <sup>11</sup>. We also note that there are points in panel (b) with very low cross sections even though they have  $m_\chi < 150$  GeV, which also have no counterparts in the CMSSM. These points associated with the funnel and their cross sections have been scaled down due to the low relic density in that region.

A new feature seen in this plot is the near-vanishing of the spin-dependent cross section when  $m_\chi = 350$  GeV. This feature is associated with the funnel region and this group of points all have cross sections substantially lower than those of the focus-point region as remarked above. However, near  $m_\chi = 350$  GeV there is the possibility for a complete cancellation in Eq. (31) when the spin contribution from up quarks cancels that due to down and strange quarks for the values in Eq. (33). While the exact position of the cancellation is sensitive to the values of the spin matrix elements adopted, the existence of the cancellation is quite robust. Of course, in this case the cross section for the scattering on neutrons will not exhibit a cancellation at the same place.

Panels (c) and (d) of Fig. 4 show a corresponding analysis for  $\tan\beta = 50$ . We first observe that there is no longer any substantial focus-point region, and we do not display in panel (c) the CMSSM contour, which lies very close to the boundary of the region where electroweak symmetry breaking is possible. We see that much of the plane is consistent with the apparent anomaly in the value of  $g_\mu - 2$ . At the larger value of  $\tan\beta$ , the branching ratio for  $B_s \rightarrow \mu^+ \mu^-$  is substantially larger, and the current limit [53] on the  $B_s \rightarrow \mu^+ \mu^-$  branching ratio of  $5.8 \times 10^{-8}$  excludes points with  $m_A < 370 - 400$  GeV (depending on the value of  $m_{1/2}$ ), as shown by the blue dotted curve. In this case, this limit is stronger than that due to the Higgs mass and excludes the lower part of the funnel and, as a consequence, neutralino masses  $\lesssim 200$  GeV.

Even though spin-independent cross sections from the funnel region are slightly boosted at large  $\tan\beta$ , much of the funnel remains out of reach of direct detection experiments, as this region is above the solid green contour corresponding to  $\sigma_p = 5 \times 10^{-8}$  pb. Moreover, the absence of a focus-point region for  $\tan\beta = 50$  removes a prospective source of points with larger cross sections. Complementary collider searches and confirmation from astrophysical indirect dark matter observations may be needed to discover dark matter if the relic density of neutralinos obtains a cosmologically-acceptable value through enhanced annihilations near a direct-channel pole. However, a good portion of the funnel (corresponding to acceptable  $g_\mu - 2$ ) is within the dashed green contour, and hence has a cross section above  $10^{-9}$  pb.

Fig. 5 shows how the  $(m_A, m_{1/2})$  plane changes if we decrease  $m_0$  to 100 GeV, which is close to the best fit found for the NUHM1 [52], from the value  $m_0 = 500$  GeV studied in Fig. 4. The most obvious effects in panel (a) are that the region where the stau and/or selectron/smuon is lighter than the lightest neutralino descends from  $m_{1/2} \sim 1900$  GeV to  $m_{1/2} \sim 500$  GeV. The  $b \rightarrow s\gamma$  and  $m_h$  constraints also become more aggressive, with the result that most of the points allowed by WMAP are in a coannihilation strip where  $m_{1/2} \sim 420$  GeV, corresponding to  $m_\chi \sim 200$  GeV - which is favoured by  $g_\mu - 2$ , moreover.

---

<sup>11</sup>We note these points also have  $m_h < 114$  GeV and are within the solid green contour in panel (a) at very low values of  $m_{1/2}$  and  $m_A$ .

There are, however, some points at both larger and smaller  $m_{1/2}$  in the rapid-annihilation funnel, and also a few points in a focus-point region close to the boundary of consistent electroweak symmetry breaking. We see in panel (b) of Fig. 5 that there is a wide range of possible values of the spin-independent cross section, particularly for small  $m_\chi$  where  $m_h < 114$  GeV. Points with  $m_\chi < 150$  GeV and such low cross sections which are associated with the funnel have no analogues in the CMSSM.

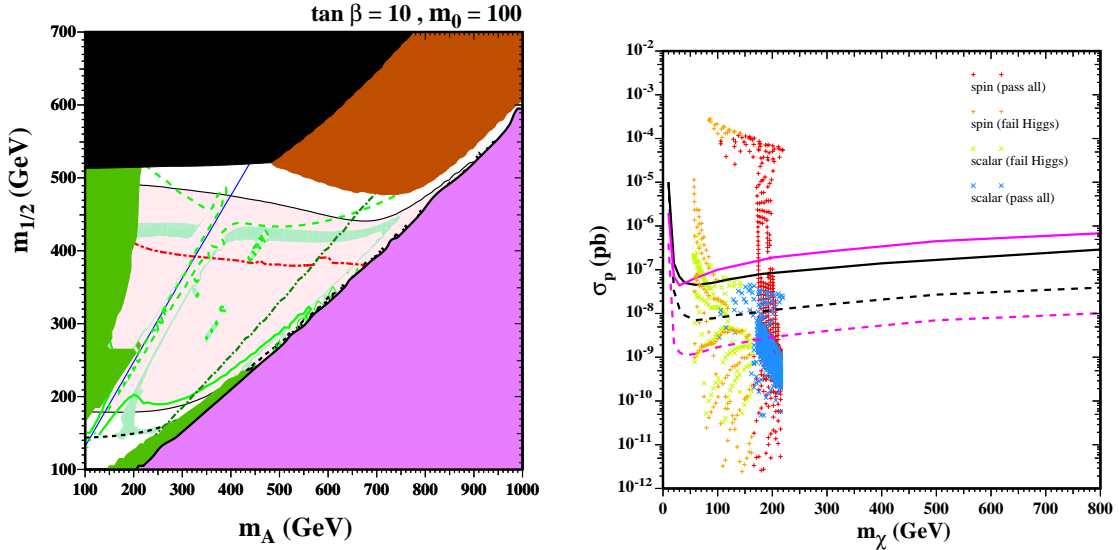


Figure 5: Panel (a) shows the NUHM1 ( $m_A, m_{1/2}$ ) planes for  $m_0 = 100$  GeV and  $\tan \beta = 10$ . Panel (b) shows the corresponding neutralino-nucleon elastic scattering cross sections as functions of neutralino mass.

### 4.3 The NUHM1 with $\mu$ as a free parameter

Fig. 6(a) shows a  $(\mu, m_{1/2})$  plane for  $\tan \beta = 10$  and  $m_0 = 500$  GeV. We see in panel (a) that  $b \rightarrow s\gamma$  excludes a region at small  $m_{1/2}$  for  $\mu < 0$ , and that the Higgs constraint excludes points with low  $m_{1/2}$  and  $\mu > 0$  in both the crossover strip and the rapid-annihilation funnel (which lies close to the electroweak vacuum boundary in this case). The intersection of the CMSSM contour with regions of acceptable relic density occurs only at very low  $m_{1/2}$ , in regions already excluded by the Higgs constraint (and also by  $b \rightarrow s\gamma$  for  $\mu < 0$ ).

The largest cross sections excluded by  $\text{BR}(b \rightarrow s\gamma)$  come from points in or between the vee-shaped crossover strips. As the  $\chi$ -nucleon scattering cross sections are smaller for  $\mu < 0$  than for  $\mu > 0$ <sup>12</sup>, the cross sections in these excluded regions are lower by more than an order of magnitude than those in regions with  $\mu > 0$  that are still allowed. Even between the

<sup>12</sup>For this reason, the upper limit on the scalar cross section is larger for  $\mu > 0$  than for  $\mu < 0$ , resulting in the lower “shadow” edge in panel (b).

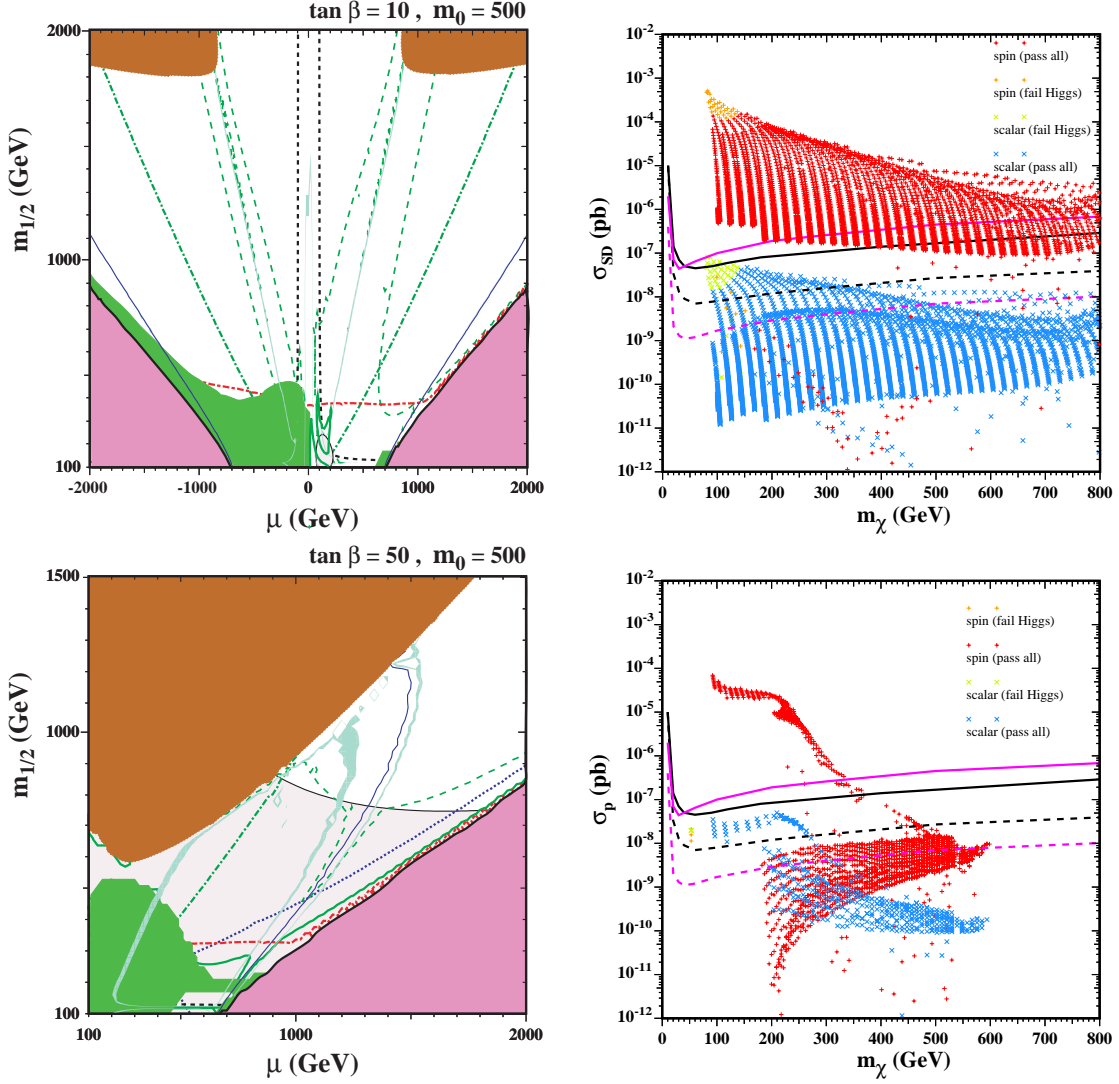


Figure 6: Panels (a) and (c) show the NUHM1  $(\mu, m_{1/2})$  planes for  $m_0 = 500$  GeV,  $\tan \beta = 10$  and 50. Panels (b) and (d) show the corresponding neutralino-nucleon elastic scattering cross sections as functions of neutralino mass.

crossover strips, at lower  $|\mu|$  where the relic density is below the WMAP range, the scaled cross sections are typically a few  $\times 10^{-8}$  pb. The largest cross sections shown in panel (b) of Fig. 6 come from points where the relic density is within the WMAP range (and therefore need no rescaling) and at low  $m_{1/2}$ , and a few of these points are in fact already excluded by CDMS II. The funnel region, as has been previously noted, gives rise to rather low spin-independent neutralino-nucleon cross sections, even at low  $m_\chi$ . A XENON100-type detector would be sensitive to the entire crossover strip region shown here for  $\mu > 0$ , and much of

that for  $\mu < 0$ , if neutralinos make up all the dark matter. We note in Fig. 6(b) the existence of points with  $100 \text{ GeV} < m_\chi < 200 \text{ GeV}$  with spin-independent cross sections  $\sim 10^{-11} \text{ pb}$ , much smaller than those found in the CMSSM for this range of masses.

In panels (c) and (d) of Figure 6, for  $\tan \beta = 50$  and  $m_0 = 500 \text{ GeV}$ , the stau LSP region has intruded so far into the parameter space that the coannihilation strip at its boundary joins the crossover strip to the rapid-annihilation funnel. The funnel itself is deformed and broadened significantly, leaving a significant region within the funnel walls where the relic density of neutralinos is below the WMAP range. Much of the funnel is favoured by  $g_\mu - 2$ . The CMSSM contour crosses regions of acceptable relic density at very low  $\mu$  and  $m_\chi$ , in an area excluded by  $b \rightarrow s\gamma$  and the Higgs mass constraint, and again near the boundary of the stau LSP region, where  $m_\chi \sim 400 \text{ GeV}$ . The largest cross sections, which occur at low  $m_\chi$ , are excluded both by  $b \rightarrow s\gamma$  and by present limits on direct detection cross sections<sup>13</sup>. While some of the coannihilation strip may be probed in the future, cross sections in the focus-point region become as low as  $\sim 10^{-10} \text{ pb}$  when the relic density is within the WMAP range. In panel (c), the large value of  $\tan \beta$  again leads to a sizeable contribution to  $B_s \rightarrow \mu^+ \mu^-$ . Points below the blue dotted curve are above the current experimental constraint of  $5 \times 10^{-8}$  [53].

In the  $(\mu, m_{1/2})$  plane for  $\tan \beta = 10$  and  $m_0 = 100 \text{ GeV}$ , shown in Fig. 7(a), a combination of the electroweak vacuum constraint, the  $\chi$  LSP constraint and  $b \rightarrow s\gamma$  excludes almost all the half-plane with  $\mu < 0$ . On the other hand, more points survive for  $\mu > 0$ , in the region bounded by the  $\chi$  LSP constraint, the LEP Higgs constraint and the LEP chargino constraint. The surviving points have spin-independent cross sections below the current upper limits, though many points with  $m_\chi < 400 \text{ GeV}$  should be accessible to future experiments. We note that there are a few points with  $m_h < 114 \text{ GeV}$  that are already excluded by XENON10 and particularly CDMS II. On the other hand, there are some points in panel (b) with very low scalar cross sections which arise from regions where the relic density is rather low (eg. in most of the region above the WMAP strip found at  $m_{1/2} = 450 \text{ GeV}$ ) and the cross section has been scaled. There is also a very sharp downturn in the spin-dependent cross section at  $m_\chi \sim 200 \text{ GeV}$  with values much smaller than in the CMSSM. This is due to a cancellation similar to the one seen in Fig. 4 between the up, down and strange contributions.

## 4.4 Summary

Fig. 8 is a pair of scatter plots displaying the potential ranges of (a) the spin-independent and (b) the spin-dependent dark matter cross sections in the NUHM1. Comparing with the corresponding plots for the CMSSM in Fig. 1, we note that the spin-independent cross section in the NUHM1 may be up to an order of magnitude larger for  $m_\chi > 300 \text{ GeV}$ . We also note the appearance of points in the NUHM1 with  $m_\chi < 200 \text{ GeV}$  and low spin-independent cross sections  $\sim 10^{-10} \text{ pb}$ . Similar features are present for the spin-dependent cross sections: in the NUHM1 this may be  $\sim 10^{-6} \text{ pb}$  for  $m_\chi > 500 \text{ GeV}$ , whereas values in the CMSSM

<sup>13</sup>The range of  $m_\chi$  in panel (d) is restricted by the range of  $m_{1/2}$  shown in panel (c).

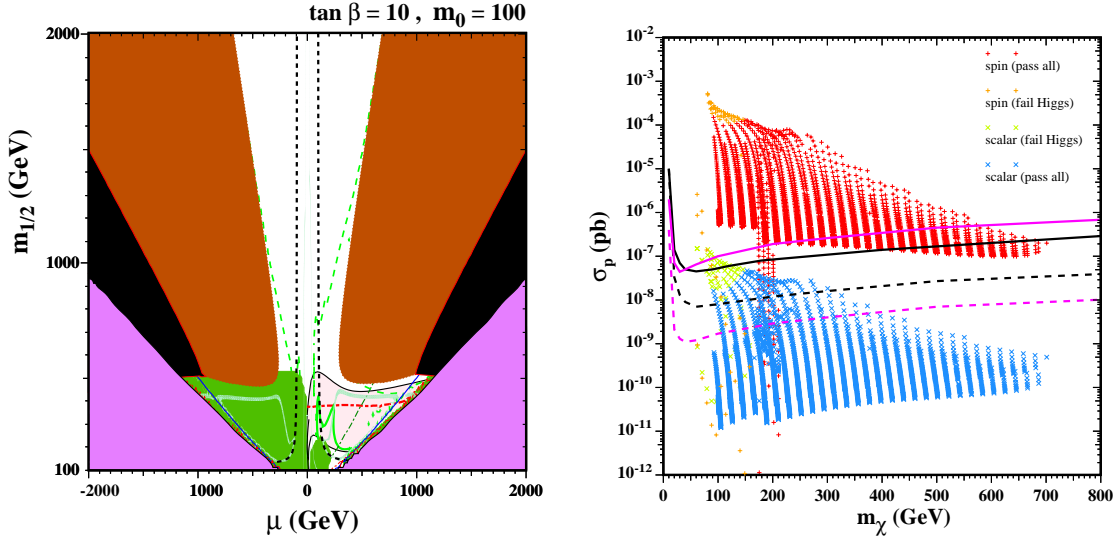


Figure 7: Panel (a) shows the NUHM1  $(\mu, m_{1/2})$  plane for  $m_0 = 100$  GeV and  $\tan \beta = 10$ . Panel (b) shows the corresponding neutralino-nucleon elastic scattering cross sections as functions of neutralino mass.

are an order of magnitude lower. Also, the NUHM1 allows the possibility of much lower spin-dependent cross sections for  $m_\chi < 300$  GeV than are attained in the CMSSM.

The points with large cross sections at large  $m_\chi$  are generally those with relatively large Higgsino components. In the CMSSM, this is possible only in focus-point regions that have relatively small  $m_\chi$ . However, in the NUHM1 there are focus-point regions extending to larger  $m_\chi$ , and there are also other cross-over regions where the LSP has a relatively large Higgsino component. Relatively low cross sections may occur in the NUHM1 at points with relatively large values of  $m_0$  or in the funnel regions due to the scaling applied when the relic density is small, as was illustrated in some of the sample planes discussed earlier.

## 5 NUHM2 Models

As already discussed, the NUHM2 has two parameters in addition to those already present in the CMSSM, which may be transposed into free choices of both the quantities  $m_A$  and  $\mu$ . The relatively large number renders complex a systematic survey of the NUHM2 parameter space. We restrict ourselves here to studies of a few parameter planes whose features we compare with the CMSSM and NUHM1. See [6], for further discussions of direct detection cross sections in the NUHM2.

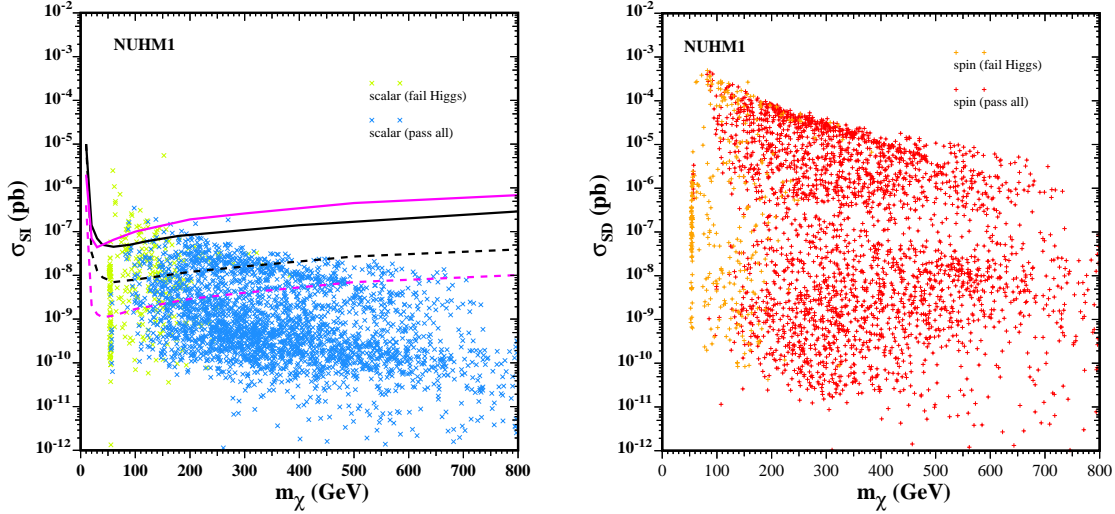


Figure 8: Panels (a) and (b) show the entire potential ranges in the NUHM1 of the scalar and spin-dependent neutralino-nucleon cross sections, respectively, as functions of neutralino mass. In both plots, we scan  $5 \leq \tan \beta \leq 55$ ,  $0 \leq m_{1/2} \leq 2000$  GeV,  $100$  GeV  $\leq m_0 \leq 2000$  GeV, and  $-3m_{1/2} \leq A_0 \leq 3m_{1/2}$ . The common GUT-scale value of  $m_1 = m_2$  is in the range  $(-2000, 2000)$  GeV.

## 5.1 Sample $(m_{1/2}, m_0)$ Plane

We first display in Fig. 9 a sample  $(m_{1/2}, m_0)$  plane with  $\tan \beta = 10$  and fixed  $m_A = 500$  GeV and  $\mu = 500$  GeV, which reveals a couple of new features. As in the CMSSM, there is a region in panel (a) at large  $m_{1/2}$  and small  $m_0$  which is forbidden because the lighter stau is the LSP. Just above this forbidden region, as in the CMSSM, there is a stau-coannihilation strip. However, jutting up from this strip at  $m_{1/2} \sim 600$  GeV and  $\sim 950$  GeV, there are vertical strips where the relic  $\chi$  density falls within the WMAP range. The double strips at  $m_{1/2} \sim 600$  GeV form a rapid-annihilation funnel on either side of the line (indicated in solid blue) where  $m_A = 2m_\chi$ . Such funnels appear only at large  $\tan \beta$  in the CMSSM, but the freedom to choose different values of  $m_A$  in the NUHM2 permits the appearance of a rapid-annihilation funnel also at the low value  $\tan \beta = 10$  shown here. The other vertical WMAP strip appears because, as  $m_{1/2}$  increases relative to  $\mu$  which is fixed here, the Higgsino fraction in the lightest neutralino  $\chi$  increases, which in turn increases the annihilation rate and hence decreases the relic density, resulting in this case in a crossover region when  $m_{1/2} \sim 950$  GeV. At slightly higher  $m_{1/2} = 1020$  GeV, there is a rapid coannihilation pole (through  $Z$ -exchange) between the lightest and next-to-lightest neutralinos resulting in a narrow region with suppressed relic density and hence a suppressed scalar cross section.

These novel regions are clearly visible in panel (b) of Fig. 9. The elastic scattering cross sections do not vary rapidly as  $m_\chi$  increases, until the funnel region at  $m_\chi \sim 250$  GeV is

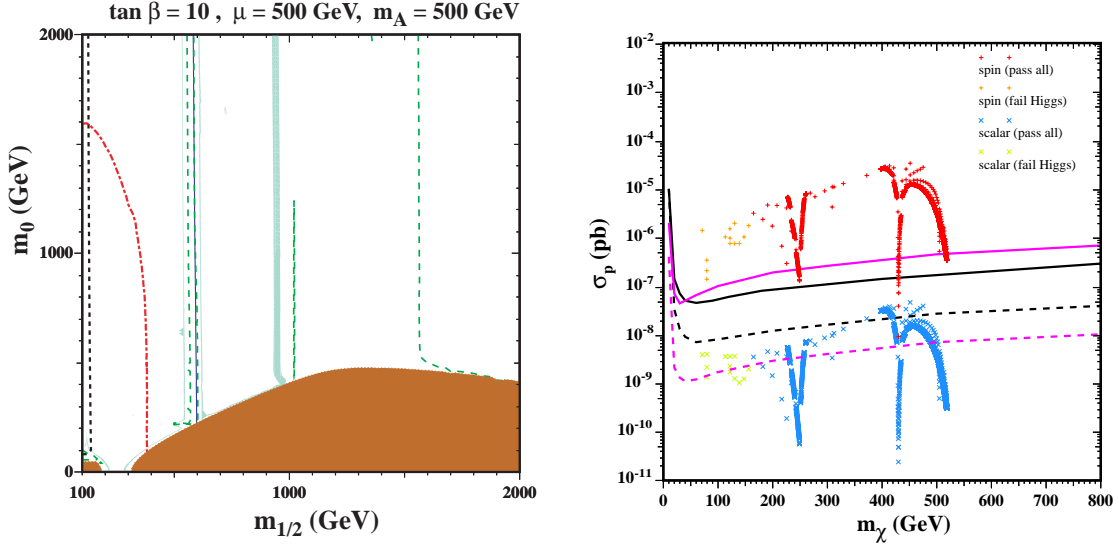


Figure 9: *Panel (a) shows the NUHM2  $(m_{1/2}, m_0)$  plane for  $m_A = 500$  GeV,  $\mu = 500$  GeV and  $\tan\beta = 10$ . Panel (b) shows the corresponding neutralino-nucleon elastic scattering cross sections as functions of neutralino mass.*

reached. The vee-shaped suppression in the cross section arises from the increasing value of  $m_0$  as one rises up the funnel. The two sides of the funnel approach each other as  $m_0$  increases, eventually joining together and resulting in a minimum value  $\sigma_{SI} \sim 5 \times 10^{-11}$  pb where the two sides of the funnel meet (at a value of  $m_0 > 2000$  GeV, and hence invisible in panel (a) of Fig. 9). After this excitement, the cross section continues to rise gradually as one follows the coannihilation strip, until the crossover strip is reached at  $m_\chi \sim 400$  GeV. Here the cross section decreases again as  $m_0$  increases, to values even smaller than in the rapid-annihilation funnel, before rising again and finally declining towards the end of the coannihilation strip. Note that the entire region to the right of the transition strip is viable, albeit with a relic density below the WMAP range. The cross section will thus be reduced due to scaling. Because the neutralino is predominantly a Higgsino here, its mass is given by  $\mu$  rather than  $m_{1/2}$  and so points at large  $m_\chi$  end in panel (b) because of our choice of fixed  $\mu$ .

## 5.2 Sample $(m_A, m_{1/2})$ Planes

Fig. 10 shows two NUHM2  $(m_A, m_{1/2})$  planes. We see in panel (a) for  $m_0 = 500$  GeV,  $\mu = 200$  GeV and  $\tan\beta = 10$  a strip with the relic density in the WMAP range that extends to large  $m_A$  at  $m_{1/2} \sim 290$  GeV. This is the transition strip, and above it, the relic density is always below the WMAP range. There are other strips below this, but they fall in a region where the chargino mass is below 104 GeV. As seen from the location of the dash-dotted red line, all of these cosmologically-preferred strips have  $m_h < 114$  GeV. In this case, the funnel



region shown by the solid blue line where  $m_A = 2m_\chi$ , occurs past the transition region and there rapid annihilation further suppresses the relic density. It is clear from the shape of this line that  $m_\chi \sim \mu = 200$  GeV for larger  $m_{1/2}$ . We see in panel (b) that the low- $m_h$  points typically have spin-independent cross sections  $\sim 10^{-7}$  pb, and are largely excluded by the XENON10 and CDMS II experiments. On the other hand, essentially all the points with  $m_h > 114$  GeV survive the direct dark matter search experiments, so far, in particular because the effective cross section is suppressed by the small relic density.

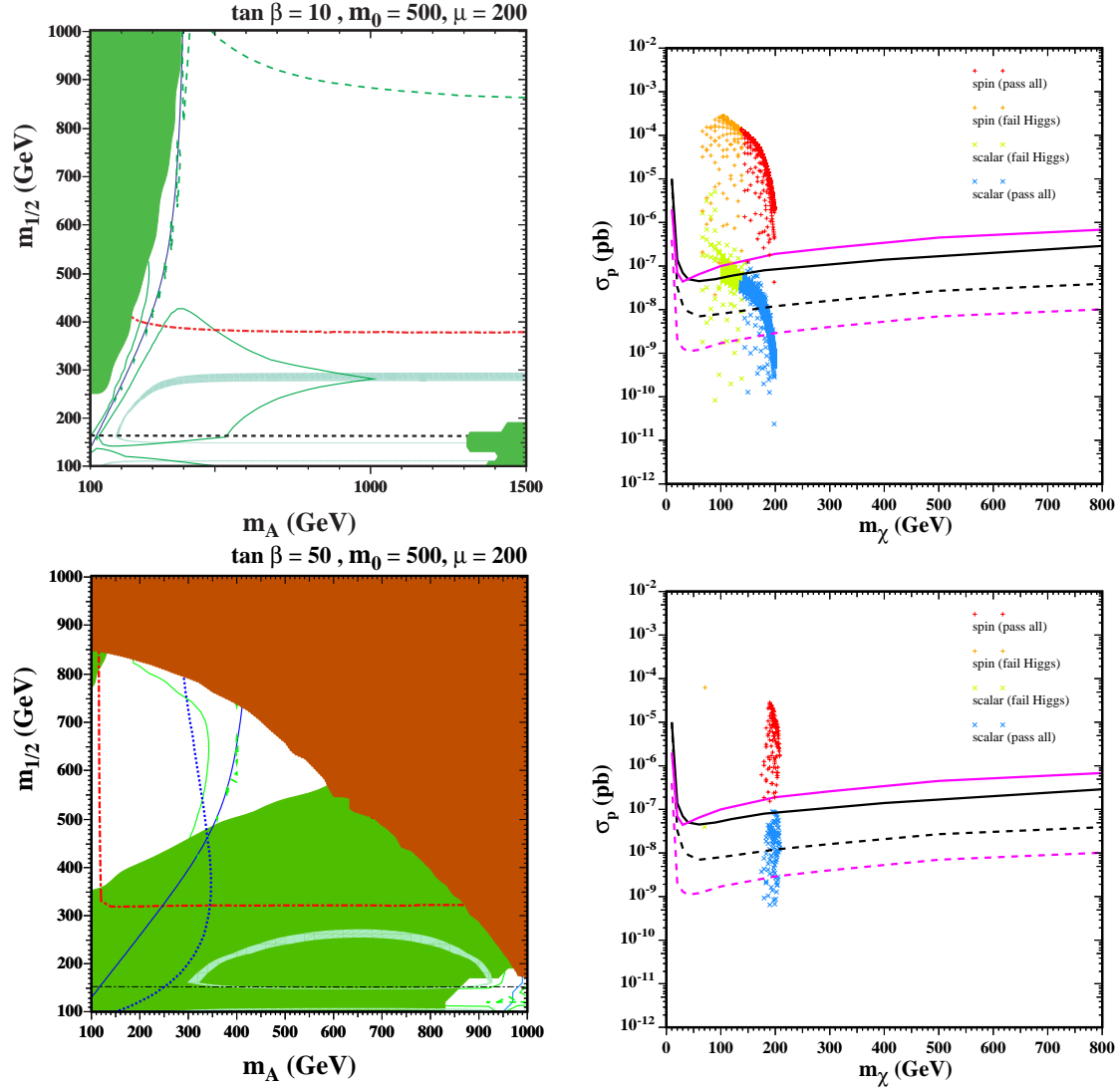


Figure 10: Panels (a) and (c) show the NUHM2  $(m_A, m_{1/2})$  planes for  $m_0 = 500$  GeV,  $\mu = 200$  GeV,  $\tan \beta = 10$  and 50. Panels (b) and (d) show the corresponding neutralino-nucleon elastic scattering cross sections as functions of neutralino mass.

Turning to the corresponding  $(m_A, m_{1/2})$  plane for  $\tan\beta = 50$ , we see a large region at large  $m_A$  and/or  $m_{1/2}$  that is excluded because the LSP is charged. There is also a large region at smaller  $m_{1/2}$  that is excluded by the  $b \rightarrow s\gamma$  constraint. At large  $\tan\beta$ , the constraint from  $B_s \rightarrow \mu^+ \mu^-$  is important, excluding values of  $m_A \lesssim 300$  GeV in this case, as shown by the dotted blue curve. Once again, although the funnel region, shown by the solid blue line where  $m_A = 2m_\chi$ , has  $m_h > 114$  GeV in between the shaded regions and to the right of the  $B_s \rightarrow \mu^+ \mu^-$  constraint, the relic density is small as this occurs past the transition region (which here is excluded by  $b \rightarrow s\gamma$ ) and the neutralino has a large Higgsino component. As seen in panel (d) of Fig. 10, all the allowed points have  $m_\chi \sim \mu = 200$  GeV. Typical spin-independent cross sections are somewhat larger than in the case  $\tan\beta = 10$ , shown previously in panel (b).

We see in Fig. 11 the evolution of these features when  $\mu = 500$  GeV, with the other parameters left unchanged. For  $\tan\beta = 10$  in panel (a), we see that the transition strip at  $m_{1/2} \approx 950$  GeV is now split by the two halves of a rapid-annihilation funnel. In contrast to Fig. 10, a portion of the funnel now lies below the transition strip and the WMAP density can be realized. Above the crossover strips, at larger  $m_{1/2}$ , the LSP becomes Higgsino-like. Only small portions of the WMAP strips have  $m_h < 114$  GeV. We see in panel (b) that the scatter plot of the spin-dependent and spin-independent cross sections has a feature at  $m_\chi \sim 430$  GeV, corresponding to the opening out of the rapid-annihilation funnel. The points at larger  $m_\chi$  have relatively large spin-independent cross sections, higher than in the CMSSM for similar values of  $m_\chi$ , reflecting the Higgsino nature of the LSP in these cases.

Turning now to panel (c) of Fig. 11, for  $\tan\beta = 50$ , we see again the increased importance of the neutralino LSP and  $b \rightarrow s\gamma$  constraints and the constraint from  $B_s \rightarrow \mu^+ \mu^-$  excluding small values of  $m_A$ . We also see the WMAP strips on either side of the solid blue line where  $m_A = 2m_\chi$ , and notice that although almost all of them have  $m_h > 114$  GeV only the upper part of the funnel is allowed by  $B_s \rightarrow \mu^+ \mu^-$ . The would-be transition strip has been pushed into the region with a charged LSP. The corresponding values of  $m_\chi \sim 250$  GeV, as seen in panel (c) of Fig. 11, and the spin-independent cross section may be as large as  $\sim 10^{-7}$  pb, namely considerably larger than in the CMSSM, but decreasing for points with a low relic density.

### 5.3 Sample $(\mu, m_{1/2})$ Planes

Fig. 12(a) displays the NUHM2  $(\mu, m_{1/2})$  plane for  $m_0 = 500$  GeV,  $m_A = 500$  GeV and  $\tan\beta = 10$ . Highly visible at large  $m_{1/2}$  are regions excluded by the neutralino LSP requirement. In the dark (very dark) shaded regions, the LSP is the stau (selectron/smuon). Much of the remaining  $\mu < 0$  half-plane is excluded by  $b \rightarrow s\gamma$ , while the lower part of the  $\mu > 0$  half-plane with  $m_{1/2} < 300$  GeV has  $m_h < 114$  GeV. Apart from a very small section of a crossover strip near  $\mu \sim -500$  GeV and  $m_{1/2} \sim 1200$  GeV, the WMAP density range is attained only in the  $\mu > 0$  half-plane. This occurs in a rapid-annihilation funnel on either side of the blue line where  $m_A = 500$  GeV =  $2m_\chi$ , and along a crossover strip extending to higher (and somewhat lower)  $m_{1/2}$ .

Panel (b) of Fig. 12 displays the corresponding dark matter scattering cross sections. We

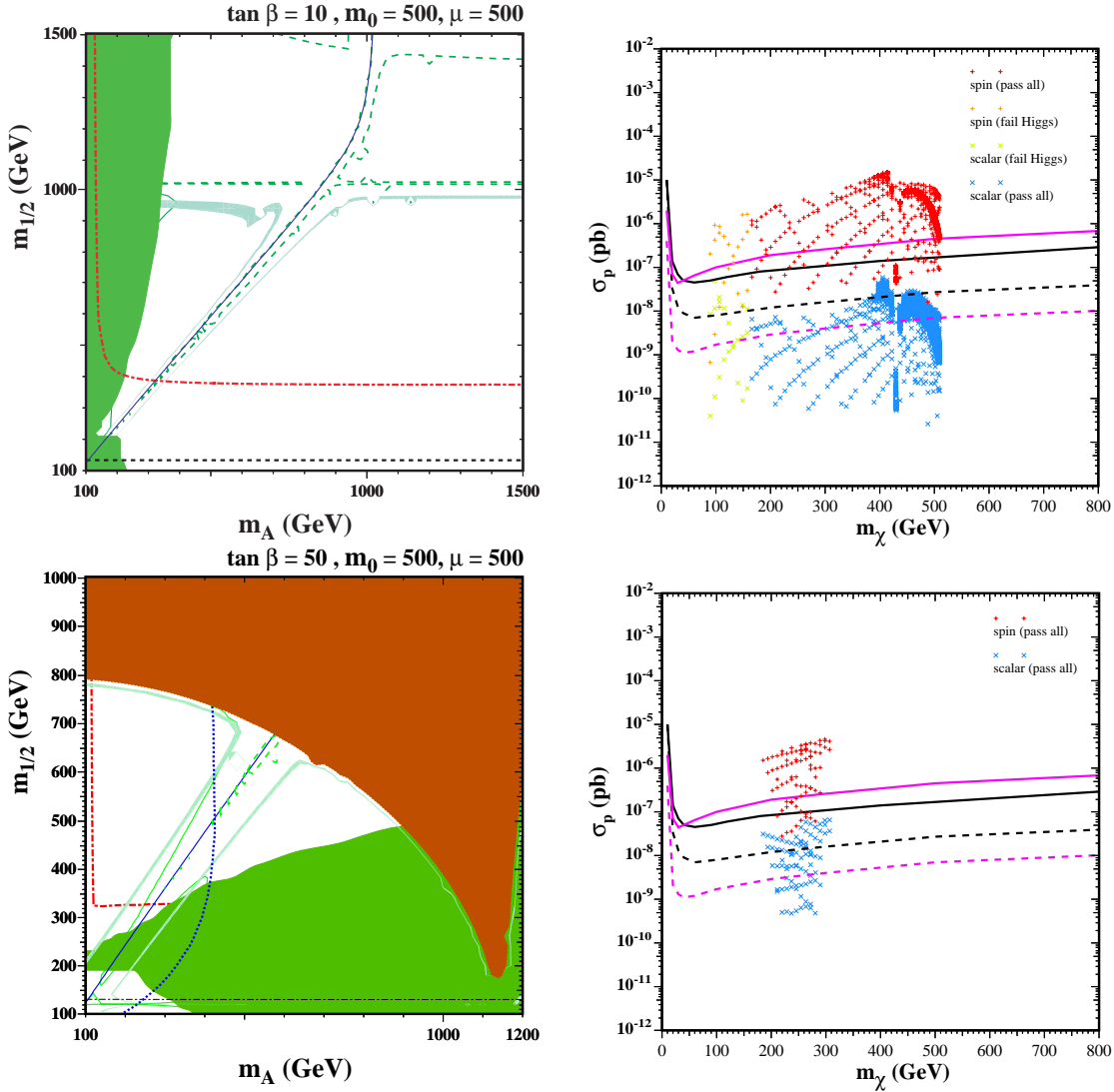


Figure 11: Panels (a) and (c) show the NUHM2  $(m_A, m_{1/2})$  planes for  $m_0 = 500$  GeV,  $\mu = 500$  GeV,  $\tan \beta = 10$  and 50. Panels (b) and (d) show the corresponding neutralino-nucleon elastic scattering cross sections as functions of neutralino mass.

see that the spin-independent cross section may be as high as  $5 \times 10^{-8}$  pb for  $m_\chi \sim 500$  GeV, to be compared with a maximum of  $\sim 10^{-9}$  pb in the CMSSM: this possibility occurs for points towards the top of the crossover strip. At small  $m_\chi$ , there are a few points with  $m_h < 114$  GeV that are excluded by the XENON10 and CDMS II experiments, which occur at the bottom end of the crossover strip. In between, for  $m_\chi \sim 250$  GeV, there is a suppression of the maximum spin-independent cross section, corresponding to the rapid-annihilation funnel extending to large  $\mu$ . Foreseen experiments should be able to cover all

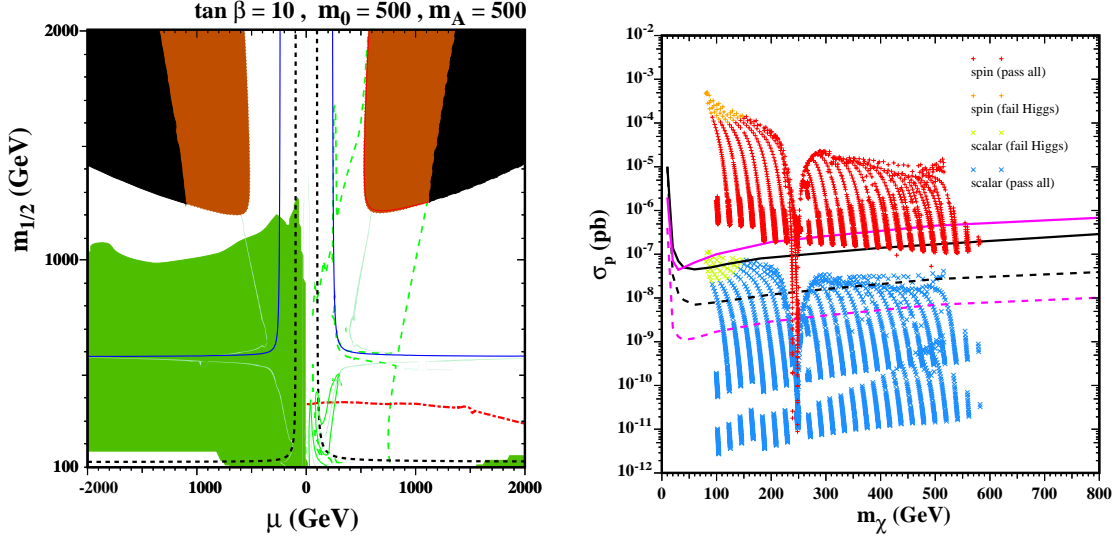


Figure 12: *Panel (a) shows the NUHM2  $(\mu, m_{1/2})$  plane for  $m_0 = 500$  GeV,  $m_A = 500$  GeV and  $\tan\beta = 10$ . Panel (b) shows the corresponding neutralino-nucleon elastic scattering cross sections as functions of neutralino mass.*

the WMAP strip except a small portion of this funnel. On the other hand, there are many points with lower effective cross sections, suppressed by the low relic density. These include some at low  $m_\chi < 200$  GeV with lower cross sections than those found in the CMSSM.

Fig. 13 displays similar NUHM2  $(\mu, m_{1/2})$  planes for  $m_0 = 1500$  GeV,  $m_A = 1000$  GeV and  $\tan\beta = 10$ . In this case, we see in panel (a) that the neutralino LSP and  $b \rightarrow s\gamma$  constraints have no effect. Almost all the half-planes for both signs of  $\mu$  have  $m_h > 114$  GeV, and the rapid-annihilation funnel has risen to  $m_{1/2} \sim 1100$  GeV, corresponding to the higher value  $m_A = 1000$  GeV. In addition to the rapid-annihilation funnels, almost all the crossover strips are allowed for both signs of  $\mu$ . Panel (b) has features rather similar to those in panel (b) of Fig. 12, with relatively large spin-independent cross sections  $\sim 10^{-8}$  pb possible for all  $m_\chi < 800$  GeV, along the crossover strips, and dips around  $m_\chi = 500$  GeV, corresponding to the rapid-annihilation funnels. As in the previous figure, low effective cross sections are again possible for points with low  $m_\chi$ , if they have a suppressed relic density, as occurs between the two crossover strips for the different signs of  $\mu$ .

## 5.4 Summary

Fig. 14 displays the potential ranges of (a) the spin-independent and (b) the spin-dependent dark matter scattering rates in the NUHM2. Comparing with the corresponding plots for the CMSSM in Fig. 1, we note that the spin-independent cross section in the NUHM1 may be up to an order of magnitude larger for  $m_\chi > 300$  GeV. As discussed in the previous subsections, the neutralino LSPs at these points typically have large Higgsino components,

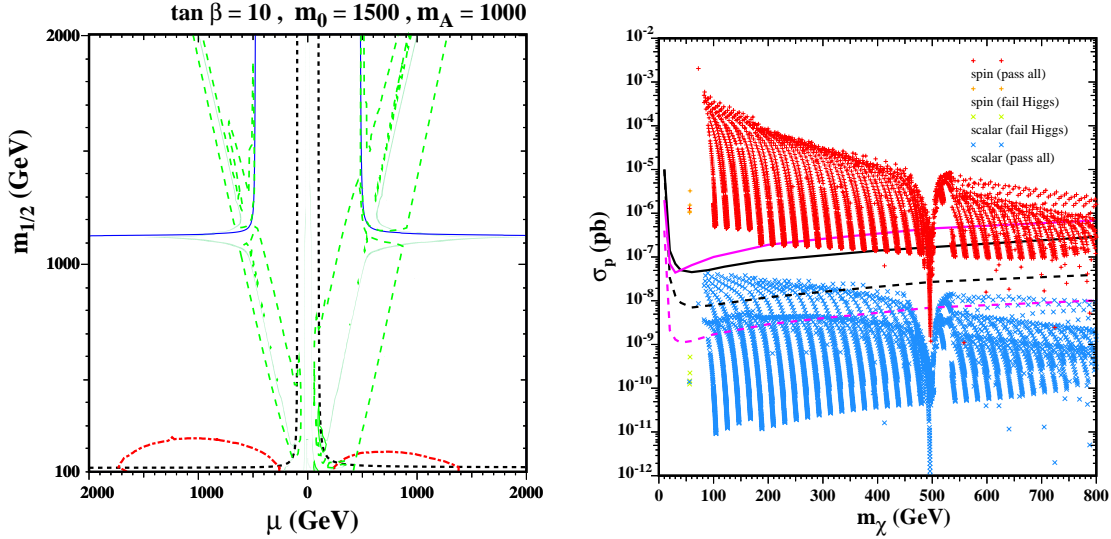


Figure 13: Panel (a) shows the NUHM2  $(\mu, m_{1/2})$  planes for  $m_0 = 1500$  GeV,  $m_A = 1000$  GeV and  $\tan \beta = 10$ . Panel (b) shows the corresponding neutralino-nucleon elastic scattering cross sections as functions of neutralino mass.

despite their large masses, and lie along crossover strips. This feature is common with the corresponding scatter plots for the NUHM1 shown in Fig. 8. We also note the appearance of NUHM2 points with  $m_\chi < 200$  GeV and low spin-independent cross sections  $\sim 10^{-10}$  pb. These points are typically in regions between the crossover strips, in regions with a very suppressed relic density. Similar features are present for the spin-dependent cross sections: in the NUHM2 this may even be  $\sim 10^{-5}$  pb for  $m_\chi > 500$  GeV, whereas values in the CMSSM are over an order of magnitude lower. Also, the NUHM2 allows the possibility of much lower spin-dependent effective cross sections for  $m_\chi < 300$  GeV than are attained in the CMSSM. These features are again similar to those found in the NUHM1.

## 6 Conclusions

We have explored in this paper the possible ranges of dark matter scattering rates in the NUHM1 and NUHM2, and compared them with the ranges attainable in the CMSSM. We have seen that the ranges that could be found in the NUHM1 and NUHM2 are both significantly broader than is possible in the CMSSM. In addition to the expectations for direct detection from broad scans, we have displayed calculated cross sections in specific slices of the NUHM1,2 parameter spaces to highlight the physical processes in  $\chi - p$  elastic scattering. Larger cross sections are possible at large  $m_\chi$ , and smaller cross sections are possible at small  $m_\chi$ . The high-mass points with the largest cross sections occur typically for points in the crossover regions with relatively large Higgsino components. Mixed Bino-

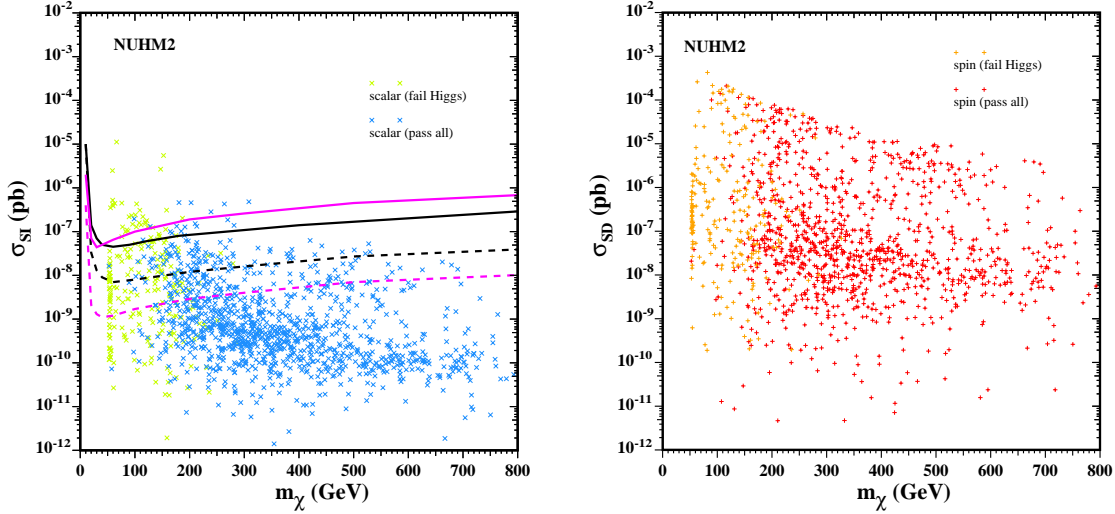


Figure 14: Panels (a) and (b) show the entire potential range of neutralino-nucleon cross sections as functions of neutralino mass for the NUHM2 for the scalar and spin dependent cross sections respectively. In both scans, we scan  $5 \leq \tan \beta \leq 55$ ,  $0 \leq m_{1/2} \leq 2000$  GeV,  $100$  GeV  $\leq m_0 \leq 2000$  GeV,  $-3m_{1/2} \leq A_0 \leq 3m_{1/2}$ , and the GUT-scale values of  $m_1$  and  $m_2$  are each in the range  $(-2000, 2000)$  GeV.

Higgsino states with the a relic density in the WMAP range may occur at much larger masses than those found in the focus-point region of the CMSSM. Several mechanisms yield points with small effective cross sections. Some points have a very suppressed relic density, e.g., points with even larger Higgsino components that are located between crossover strips. In other cases, the cross section may be suppressed because the point is in a rapid-annihilation funnel region at larger  $m_0$  and smaller  $m_{1/2}$  than is possible in the CMSSM, or in a crossover region at larger  $m_0$ , or at larger  $m_A$  or  $\mu$ .

Present direct dark matter searches for spin-independent scattering, in particular the XENON10 and CDMS II experiments, are beginning to chip away at the parameter spaces of the CMSSM, NUHM1 and NUHM2. However, most of the points excluded so far have small  $m_\chi$  and  $m_h < 114$  GeV. On the other hand, prospective searches for spin-independent scattering could be sensitive to NUHM1 or NUHM2 models with LSP masses as large as 800 GeV, the largest we have sampled, whereas they would be sensitive only to  $m_\chi < 350$  GeV within the CMSSM<sup>14</sup>. Thus, observation of spin-independent scattering by a heavy LSP would be a good diagnostic for a more complicated supersymmetric model than the CMSSM, and perhaps a hint for a neutralino with a significant Higgsino component in one of the crossover regions. Conversely, if some other experiment, e.g., at the LHC, establishes the

<sup>14</sup>Unfortunately, searches for spin-dependent dark matter scattering are still some distance away achieving the sensitivity needed to probe the classes of models discussed in this paper.

existence of a light LSP, but its spin-independent scattering is *not* seen, this could also be a hint for some model more complicated than the CMSSM in which the relic density is suppressed, e.g., by one of the mechanisms described in the previous paragraph that operate in the NUHM1 and NUHM2.

Neither the LHC experiments nor direct dark matter searches can, by themselves, tell us all we would like to know about the manner in which supersymmetry is broken. However, as we have illustrated in this paper, the combination of LHC experiments and direct dark matter searches could provide some interesting hints.

## 7 Acknowledgements

The work of K.A.O. is supported in part by DOE grant DE-FG02-94ER-40823 at the University of Minnesota. The work of P.S. is supported in part by the National Science Foundation under Grant No. PHY-0455649.

## References

- [1] J. Ellis, J.S. Hagelin, D.V. Nanopoulos, K.A. Olive and M. Srednicki, Nucl. Phys. B **238** (1984) 453; see also H. Goldberg, Phys. Rev. Lett. **50** (1983) 1419.
- [2] M. W. Goodman and E. Witten, Phys. Rev. D **31**, 3059 (1985).
- [3] K. Griest, Phys. Rev. D **38**, 2357 (1988); J. Ellis and R. Flores, Nucl. Phys. B **307**, 883 (1988); R. Barbieri, M. Frigeni and G. Giudice, Nucl. Phys. B **313**, 725 (1989); R. Flores, K.A. Olive and M. Srednicki, Phys. Lett. B **237**, 72 (1990); J. Ellis and R. Flores, Phys. Lett. B **263**, 259 (1991); J. Ellis and R. Flores, Phys. Lett. B **300**, 175 (1993); M. Drees and M. M. Nojiri, Phys. Rev. D **48**, 3483 (1993); V. Bednyakov, H.V. Klapdor-Kleingrothaus and S. Kovalenko, Phys. Rev. D **50**, 7128 (1994); R. Arnowitt and P. Nath, Phys. Rev. D **54**, 2374 (1996) [arXiv:hep-ph/9509260]; L. Bergstrom and P. Gondolo, Astropart. Phys. **5**, 263 (1996) [arXiv:hep-ph/9510252].
- [4] H. Baer and M. Brhlik, Phys. Rev. D **57**, 567 (1998) [arXiv:hep-ph/9706509]; A. Corsetti and P. Nath, Phys. Rev. D **64** (2001) 125010 [arXiv:hep-ph/0003186]; E. Accomando, R. Arnowitt, B. Dutta and Y. Santoso, Nucl. Phys. B **585**, 124 (2000) [arXiv:hep-ph/0001019]; R. Arnowitt, B. Dutta and Y. Santoso, arXiv:hep-ph/0005154.
- [5] J. Ellis, A. Ferstl and K. A. Olive, Phys. Lett. B **481**, 304 (2000) [arXiv:hep-ph/0001005]; J. Ellis, A. Ferstl and K. A. Olive, Phys. Rev. D **63**, 065016 (2001) [arXiv:hep-ph/0007113]; J. R. Ellis, A. Ferstl and K. A. Olive, Phys. Lett. B **532**, 318 (2002) [arXiv:hep-ph/0111064].
- [6] J. R. Ellis, A. Ferstl, K. A. Olive and Y. Santoso, Phys. Rev. D **67** (2003) 123502 [arXiv:hep-ph/0302032].

- [7] J. R. Ellis, J. L. Feng, A. Ferstl, K. T. Matchev and K. A. Olive, *Eur. Phys. J. C* **24**, 311 (2002) [arXiv:astro-ph/0110225].
- [8] E. A. Baltz and P. Gondolo, *Phys. Rev. Lett.* **86**, 5004 (2001) [arXiv:hep-ph/0102147];
- [9] J. L. Feng, K. T. Matchev and F. Wilczek, *Phys. Lett. B* **482** (2000) 388 [arXiv:hep-ph/0004043]; M. Drees, Y. G. Kim, T. Kobayashi and M. M. Nojiri, *Phys. Rev. D* **63**, 115009 (2001) [arXiv:hep-ph/0011359]; A. B. Lahanas, D. V. Nanopoulos and V. C. Spanos, *Mod. Phys. Lett. A* **16**, 1229 (2001) [arXiv:hep-ph/0009065]; A. B. Lahanas, D. V. Nanopoulos and V. C. Spanos, *Phys. Lett. B* **518**, 94 (2001) [arXiv:hep-ph/0107151]; Y. G. Kim, T. Nihei, L. Roszkowski and R. Ruiz de Austri, *JHEP* **0212**, 034 (2002) [arXiv:hep-ph/0208069]; M. E. Gómez and J. D. Vergados, *Phys. Lett. B* **512**, 252 (2001) [arXiv:hep-ph/0012020]; H. Baer, C. Balazs, A. Belyaev and J. O’Farrill, *JCAP* **0309**, 007 (2003) [arXiv:hep-ph/0305191].
- [10] A. Bottino, F. Donato, N. Fornengo and S. Scopel, *Phys. Rev. D* **59**, 095003 (1999) [arXiv:hep-ph/9808456]; *Phys. Rev. D* **59**, 095004 (1999) [arXiv:hep-ph/9808459]; *Phys. Rev. D* **63**, 125003 (2001) [arXiv:hep-ph/0010203]; R. Arnowitt and P. Nath, *Phys. Rev. D* **60**, 044002 (1999) [arXiv:hep-ph/9902237]; R. Arnowitt, B. Dutta and Y. Santoso, *Nucl. Phys. B* **606**, 59 (2001) [arXiv:hep-ph/0102181].
- [11] A. Bottino, F. Donato, N. Fornengo and S. Scopel, *Astropart. Phys.* **13**, 215 (2000) [arXiv:hep-ph/9909228]; *Astropart. Phys.* **18**, 205 (2002) [arXiv:hep-ph/0111229].
- [12] Y. G. Kim and M. M. Nojiri, *Prog. Theor. Phys.* **106**, 561 (2001) [arXiv:hep-ph/0104258];
- [13] J. R. Ellis, K. A. Olive, Y. Santoso and V. C. Spanos, *Phys. Rev. D* **71**, 095007 (2005) [arXiv:hep-ph/0502001].
- [14] J. R. Ellis, K. A. Olive and C. Savage, *Phys. Rev. D* **77**, 065026 (2008) [arXiv:0801.3656 [hep-ph]].
- [15] S. P. Martin, arXiv:hep-ph/9709356; J. R. Ellis, arXiv:hep-ph/9812235; K. A. Olive, arXiv:hep-ph/9911307; M. E. Peskin, arXiv:0801.1928 [hep-ph].
- [16] M. Drees and M. M. Nojiri, *Phys. Rev. D* **47**, 376 (1993) [arXiv:hep-ph/9207234]; H. Baer and M. Brhlik, *Phys. Rev. D* **53**, 597 (1996) [arXiv:hep-ph/9508321]; H. Baer and M. Brhlik, *Phys. Rev. D* **57**, 567 (1998) [arXiv:hep-ph/9706509]; V. D. Barger and C. Kao, *Phys. Rev. D* **57**, 3131 (1998) [arXiv:hep-ph/9704403]; J. R. Ellis, T. Falk, G. Ganis, K. A. Olive and M. Srednicki, *Phys. Lett. B* **510**, 236 (2001) [arXiv:hep-ph/0102098]; V. D. Barger and C. Kao, *Phys. Lett. B* **518** (2001) 117 [arXiv:hep-ph/0106189]; L. Roszkowski, R. Ruiz de Austri and T. Nihei, *JHEP* **0108**, 024 (2001) [arXiv:hep-ph/0106334]; A. B. Lahanas and V. C. Spanos, *Eur. Phys. J. C* **23**, 185 (2002) [arXiv:hep-ph/0106345]; A. Djouadi, M. Drees and J. L. Kneur, *JHEP* **0108**, 055 (2001) [arXiv:hep-ph/0107316]; U. Chattopadhyay, A. Corsetti and P. Nath, *Phys. Rev.*



- D **66**, 035003 (2002) [arXiv:hep-ph/0201001]; J. R. Ellis, K. A. Olive and Y. Santoso, New J. Phys. **4**, 32 (2002) [arXiv:hep-ph/0202110]; H. Baer, C. Balazs, A. Belyaev, J. K. Mizukoshi, X. Tata and Y. Wang, JHEP **0207**, 050 (2002) [arXiv:hep-ph/0205325]; R. Arnowitt and B. Dutta, arXiv:hep-ph/0211417.
- [17] J. R. Ellis, K. A. Olive, Y. Santoso and V. C. Spanos, Phys. Lett. B **565**, 176 (2003) [arXiv:hep-ph/0303043]; H. Baer and C. Balazs, JCAP **0305**, 006 (2003) [arXiv:hep-ph/0303114]; A. B. Lahanas and D. V. Nanopoulos, Phys. Lett. B **568**, 55 (2003) [arXiv:hep-ph/0303130]; U. Chattopadhyay, A. Corsetti and P. Nath, Phys. Rev. D **68**, 035005 (2003) [arXiv:hep-ph/0303201]; C. Munoz, Int. J. Mod. Phys. A **19**, 3093 (2004) [arXiv:hep-ph/0309346]; R. Arnowitt, B. Dutta and B. Hu, arXiv:hep-ph/0310103.
- [18] S. Dimopoulos and H. Georgi, Nucl. Phys. B **193**, 150 (1981).
- [19] D. Matalliotakis and H. P. Nilles, Nucl. Phys. B **435** (1995) 115 [arXiv:hep-ph/9407251]; M. Olechowski and S. Pokorski, Phys. Lett. B **344**, 201 (1995) [arXiv:hep-ph/9407404]; V. Berezinsky, A. Bottino, J. R. Ellis, N. Fornengo, G. Mignola and S. Scopel, Astropart. Phys. **5**, 1 (1996) [arXiv:hep-ph/9508249]; M. Drees, M. M. Nojiri, D. P. Roy and Y. Yamada, Phys. Rev. D **56**, 276 (1997) [Erratum-ibid. D **64** (1997) 039901] [arXiv:hep-ph/9701219]; M. Drees, Y. G. Kim, M. M. Nojiri, D. Toya, K. Hasuko and T. Kobayashi, Phys. Rev. D **63**, 035008 (2001) [arXiv:hep-ph/0007202]; P. Nath and R. Arnowitt, Phys. Rev. D **56**, 2820 (1997) [arXiv:hep-ph/9701301]; J. R. Ellis, T. Falk, G. Ganis, K. A. Olive and M. Schmitt, Phys. Rev. D **58**, 095002 (1998) [arXiv:hep-ph/9801445]; J. R. Ellis, T. Falk, G. Ganis and K. A. Olive, Phys. Rev. D **62** (2000) 075010 [arXiv:hep-ph/0004169]; A. Bottino, F. Donato, N. Fornengo and S. Scopel, Phys. Rev. D **63**, 125003 (2001) [arXiv:hep-ph/0010203]; S. Profumo, Phys. Rev. D **68**, 015006 (2003) [arXiv:hep-ph/0304071]; D. Cerdeno and C. Munoz, JHEP **0410** (2004) 015, hep-ph/0405057;
- [20] H. Baer, A. Mustafayev, S. Profumo, A. Belyaev and X. Tata, Phys. Rev. D **71**, 095008 (2005) [arXiv:hep-ph/0412059]. H. Baer, A. Mustafayev, S. Profumo, A. Belyaev and X. Tata, JHEP **0507** (2005) 065, hep-ph/0504001.
- [21] J. R. Ellis, K. A. Olive and P. Sandick, Phys. Rev. D **78**, 075012 (2008) [arXiv:0805.2343 [hep-ph]].
- [22] J. Ellis, K. Olive and Y. Santoso, Phys. Lett. B **539**, 107 (2002) [arXiv:hep-ph/0204192]; J. R. Ellis, T. Falk, K. A. Olive and Y. Santoso, Nucl. Phys. B **652**, 259 (2003) [arXiv:hep-ph/0210205].
- [23] J. R. Ellis, S. Heinemeyer, K. A. Olive, A. M. Weber and G. Weiglein, JHEP **0708**, 083 (2007) [arXiv:0706.0652 [hep-ph]]; J. Ellis, T. Hahn, S. Heinemeyer, K. A. Olive and G. Weiglein, JHEP **0710**, 092 (2007) [arXiv:0709.0098 [hep-ph]].
- [24] V. D. Barger, M. S. Berger and P. Ohmann, Phys. Rev. D **49** (1994) 4908 [arXiv:hep-ph/9311269].

- [25] W. de Boer, R. Ehret and D. I. Kazakov, *Z. Phys. C* **67** (1995) 647 [arXiv:hep-ph/9405342].
- [26] M. Carena, J. R. Ellis, A. Pilaftsis and C. E. Wagner, *Nucl. Phys. B* **625** (2002) 345 [arXiv:hep-ph/0111245].
- [27] L. E. Ibanez, C. Lopez and C. Munoz, *Nucl. Phys. B* **256** (1985) 218.
- [28] S. P. Martin and M. T. Vaughn, *Phys. Rev. D* **50** (1994) 2282 [arXiv:hep-ph/9311340].
- [29] T. Falk, A. Ferstl and K. A. Olive, *Phys. Rev. D* **59**, 055009 (1999) [Erratum-ibid. *D* **60**, 119904 (1999)] [arXiv:hep-ph/9806413]; T. Falk, A. Ferstl and K. A. Olive, *Astropart. Phys.* **13**, 301 (2000) [arXiv:hep-ph/9908311].
- [30] P. F. Smith and J. D. Lewin, *Phys. Rept.* **187**, 203 (1990); J. D. Lewin and P. F. Smith, *Astropart. Phys.* **6**, 87 (1996).
- [31] M. A. Shifman, A. I. Vainshtein and V. I. Zakharov, *Phys. Lett. B* **78**, 443 (1978).
- [32] A. I. Vainshtein, V. I. Zakharov and M. A. Shifman, *Sov. Phys. Usp.* **23**, 429 (1980) [*Usp. Fiz. Nauk* **131**, 537 (1980)].
- [33] H. Leutwyler, *Phys. Lett. B* **378**, 313 (1996) [arXiv:hep-ph/9602366].
- [34] C. Amsler *et al.* [Particle Data Group], *Phys. Lett. B* **667**, 1 (2008).
- [35] G. Brooijmans [CDF and D0 Collaborations], hep-ex/0005030.  
<http://www-d0.fnal.gov/public/top/top>,  
<http://www-cdf.fnal.gov/physics/new/top/results/mass/combine>.
- [36] H. Y. Cheng, *Phys. Lett. B* **219**, 347 (1989).
- [37] B. Borasoy and U. G. Meissner, *Annals Phys.* **254**, 192 (1997) [arXiv:hep-ph/9607432].
- [38] J. Gasser, H. Leutwyler and M. E. Sainio, *Phys. Lett. B* **253**, 252 (1991).
- [39] M. Knecht, *PiN Newslett.* **15**, 108 (1999) [arXiv:hep-ph/9912443].
- [40] M. E. Sainio, *PiN Newslett.* **16**, 138 (2002) [arXiv:hep-ph/0110413].
- [41] R. D. Young and A. W. Thomas, arXiv:0901.3310 [hep-lat].
- [42] Joint LEP 2 Supersymmetry Working Group, *Combined LEP Chargino Results, up to 208 GeV*,  
[http://lepsusy.web.cern.ch/lepsusy/www/inos\\_moriond01/charginos\\_pub.html](http://lepsusy.web.cern.ch/lepsusy/www/inos_moriond01/charginos_pub.html);  
 LEP Higgs Working Group for Higgs boson searches, OPAL Collaboration, ALEPH Collaboration, DELPHI Collaboration and L3 Collaboration, *Phys. Lett. B* **565** (2003) 61 [arXiv:hep-ex/0306033]. *Search for neutral Higgs bosons at LEP*, paper submitted to ICHEP04, Beijing, LHWG-NOTE-2004-01, ALEPH-2004-008, DELPHI-2004-042,

L3-NOTE-2820, OPAL-TN-744,  
[http://lephiggs.web.cern.ch/LEPHIGGS/papers/  
August2004\\_MSSM/index.html](http://lephiggs.web.cern.ch/LEPHIGGS/papers/August2004_MSSM/index.html).

- [43] S. Chen *et al.* [CLEO Collaboration], *Phys. Rev. Lett.* **87** (2001) 251807 [arXiv:hep-ex/0108032]; P. Koppenburg *et al.* [Belle Collaboration], *Phys. Rev. Lett.* **93** (2004) 061803 [arXiv:hep-ex/0403004]. B. Aubert *et al.* [BaBar Collaboration], arXiv:hep-ex/0207076; E. Barberio *et al.* [Heavy Flavor Averaging Group (HFAG)], arXiv:hep-ex/0603003.
- [44] G. Bennett *et al.* [The Muon g-2 Collaboration], *Phys. Rev. Lett.* **92** (2004) 161802, hep-ex/0401008; G. Bennett *et al.* [The Muon g-2 Collaboration], *Phys. Rev. D* **73** (2006) 072003 [arXiv:hep-ex/0602035].
- [45] J. Dunkley *et al.* [WMAP Collaboration], *Astrophys. J. Suppl.* **180**, 306 (2009) [arXiv:0803.0586 [astro-ph]]; E. Komatsu *et al.* [WMAP Collaboration], *Astrophys. J. Suppl.* **180**, 330 (2009) [arXiv:0803.0547 [astro-ph]].
- [46] Z. Ahmed *et al.* [CDMS Collaboration], *Phys. Rev. Lett.* **102**, 011301 (2009) [arXiv:0802.3530 [astro-ph]].
- [47] J. Angle *et al.* [XENON Collaboration], *Phys. Rev. Lett.* **100**, 021303 (2008) [arXiv:0706.0039 [astro-ph]].
- [48] E. Aprile, L. Baudis and f. t. X. Collaboration, arXiv:0902.4253 [astro-ph.IM].
- [49] *SuperCDMS Development Project*, Fermilab Proposal 0947, October 2004.
- [50] H. S. Lee. *et al.* [KIMS Collaboration], *Phys. Rev. Lett.* **99**, 091301 (2007) [arXiv:0704.0423 [astro-ph]].
- [51] S. Heinemeyer, W. Hollik and G. Weiglein, *Comput. Phys. Commun.* **124** (2000) 76 [arXiv:hep-ph/9812320]; S. Heinemeyer, W. Hollik and G. Weiglein, *Eur. Phys. J. C* **9** (1999) 343 [arXiv:hep-ph/9812472]; G. Degrassi, S. Heinemeyer, W. Hollik, P. Slavich and G. Weiglein, *Eur. Phys. J. C* **28** (2003) 133 [arXiv:hep-ph/0212020].; M. Frank, T. Hahn, S. Heinemeyer, W. Hollik, H. Rzehak and G. Weiglein, *JHEP* **0702** (2007) 047 [arXiv:hep-ph/0611326].
- [52] O. Buchmueller *et al.*, *JHEP* **0809**, 117 (2008) [arXiv:0808.4128 [hep-ph]].
- [53] T. Aaltonen *et al.* [CDF Collaboration], *Phys. Rev. Lett.* **100**, 101802 (2008) [arXiv:0712.1708 [hep-ex]].